

# Magic numbers for superheavy nuclei in relativistic continuum Hartree-Bogoliubov theory

W. Zhang,<sup>1</sup> J. Meng,<sup>1,2,3,\*</sup> S. Q. Zhang,<sup>1</sup> L. S. Geng,<sup>1,4</sup> and H. Toki<sup>4</sup>

<sup>1</sup>*School of Physics, Peking University, Beijing 100871*

<sup>2</sup>*Institute of Theoretical Physics, Chinese Academy of Science, Beijing 100080*

<sup>3</sup>*Center of Theoretical Nuclear Physics,  
National Laboratory of Heavy Ion Accelerator, Lanzhou 730000*

<sup>4</sup>*Research Center for Nuclear Physics (RCNP),  
Osaka University, Ibaraki, Osaka, 567-0047, Japan*

(Dated: July 5, 2018)

## Abstract

The magic proton and neutron numbers are searched in the superheavy region with proton number  $Z=100 - 140$  and neutron number  $N= (Z+30) - (2Z+32)$  by the relativistic continuum Hartree-Bogoliubov (RCHB) theory with interactions NL1, NL3, NLSH, TM1, TW99, DD-ME1, PK1, and PK1R. Based on the two-nucleon separation energies  $S_{2p}$  and  $S_{2n}$ , the two-nucleon gaps  $\delta_{2p}$  and  $\delta_{2n}$ , the shell correction energies  $E_{shell}^p$  and  $E_{shell}^n$ , the pairing energies  $E_{pair}^p$  and  $E_{pair}^n$ , and the pairing gaps  $\Delta_p$  and  $\Delta_n$ ,  $Z=120, 132, \text{ and } 138$  and  $N=172, 184, 198, 228, 238, \text{ and } 258$  are suggested to be the magic numbers within the present approach. The  $\alpha$ -decay half-lives are also discussed. In addition, the potential energy surfaces of possible doubly magic nuclei are obtained by the deformation-constrained relativistic mean field (RMF) theory, and the shell effects stabilizing the nuclei are investigated. Furthermore, the formation cross sections of  ${}_{172}^{292}\text{120}$  and  ${}_{184}^{304}\text{120}$  at the optimal excitation energy are estimated by a phenomenological cold fusion reactions model with the structure information extracted from the constrained RMF calculation.

PACS numbers: 21.10.Dr, 21.60.Jz, 24.10.Jv, 24.60.Dr, 27.90.+b

---

\*e-mail: mengj@pku.edu.cn

## I. INTRODUCTION

The structure of heavy and superheavy nuclei has been an interesting field of nuclear physics research during the last decades. Since the stability of superheavy nuclei is mainly determined by the shell effects, it is important to find out the regions in the  $(Z, N)$  plane where the shell effects are strong and the long lifetime of the superheavy nuclei can be expected. Exploring the limit of nuclear charge and mass is a long-term goal of nuclear physics, and searching for the superheavy nuclei has been enlivened by the hope of creating nuclei with masses and charges much larger than those we are familiar with. The limit on stability in superheavy nuclear region is essential for understanding not only the nuclear structure, but also the structure of the stars and the evolution of the universe. In the classical droplet theory, the superheavy nuclei can not exist due to their large Coulomb potentials. It is the shell effects that play a major role for the very existence of nuclei with magic numbers and provide higher stability and also higher abundance as compared to their neighbors. A semblance of the same would work also for superheavy nuclei, if there were magic numbers in this region. Consequently, these nuclei will be guarded against a faster decay by fission as compared to their non-magic counterparts, and have more opportunities to be bound.

The pioneer theoretical work on the superheavy elements can be found in the 1960's [1, 2, 3, 4]. A series of calculations based on the macroscopic-microscopic method (Nilsson-Strutinsky approach) with the folded-Yukawa deformed single-particle potential [5] and with the Woods-Saxon deformed single-particle potential [6, 7, 8] are successful in reproducing the well-known  $\alpha$ -decay half-lives of heavy elements. The existence of island of superheavy nuclei would be separated in neutron and proton number from the known heavy elements by a region of much higher instability. Experimentally, the superheavy elements up to  $Z=116$  are synthesized or claimed to be synthesized [9, 10, 11, 12, 13, 14, 15, 16, 17, 18, 19] by different heavy ion reaction types including the cold fusion reactions. The usual view is that although these isotopes are very heavy indeed, they are not examples of the originally sought island of superheavy elements.

There is no consensus among different theories with regard to the center of the island of superheavy nuclei. Based upon phenomenological models such as finite-range droplet model (FRDM), the shell closure were predicted at  $Z=114$  and  $N=184$  [20]. Additionally,

the FRDM also predicts larger shell gaps at  $Z=104, 106, 108, 110$  and at  $N=162, 164$  [20]. Based on Nilsson-Strutinsky scheme, a similar pattern of deformed nuclei have been predicted about  $Z=108$  and  $N=162$  as in FRDM [8, 21]. However, the main obstacle is the question whether the macroscopic approaches which apply to the region of  $\beta$ -stability line can be extrapolated to the superheavy nuclei. Recently, microscopic calculations [22, 23, 24, 25, 26, 27, 28, 29] are also attempted in describing the superheavy nuclei. In the framework of relativistic Hartree-Bogoliubov (RHB) theory, calculation with a finite-range pairing force of Gogny interaction D1 and effective interaction NLSH show that  $Z=114$  and  $N=160, N=166, N=184$  exhibit stability compared to their neighbors and indications for a doubly magic character at  $Z=106$  and  $N=160$  are also observed [23]. The Skyrme Hartree-Fock (SHF) method with interactions SkP and SLy7 predicts magic numbers at  $Z=126$  and  $N=184$ , and also predicts the increased stability due to the deformed shell effects at  $N=162$  [24]. Considering non-relativistic SHF effective interactions SkM\*, SkP, SLy6, SkI1, SkI3, SkI4 and relativistic mean field (RMF) effective interactions PL-40, NLSH, NL-Z, TM1, Ref. [25] gave the doubly magic spherical nuclei  ${}_{184}114$ ,  ${}_{172}120$  and  ${}_{184}126$  based on two-nucleon gaps  $\delta_{2p}$  and  $\delta_{2n}$ . The common point of such studies is that the magic numbers depend on effective interactions. The study of superheavy nuclei remains a challenge for interaction, which have to be rigorously tested by a wide variety of nuclear properties throughout the periodic table.

The extrapolation towards superheavy nuclei challenges the predictive power of nuclear structure models. The relativistic mean field (RMF) theory has achieved a great success in describing many nuclear phenomena [30] and it is believed as one of the best candidates for application to superheavy nuclei. The relativistic continuum Hartree-Bogoliubov (RCHB) theory is the extension of the RMF and the Bogoliubov transformation in the coordinate representation [31]. As the RCHB formalism allows for the proper description of the coupling between the bound states and the continuum by the pairing force, therefore it is suitable not only for stable nuclei but also for the nuclei near the drip line [32, 33, 34, 35, 36]. The RCHB theory has shown a remarkable success in the description of nuclei with unusual  $N/Z$  ratio, e.g., the halo in  ${}^{11}\text{Li}$  [32] and the description of the giant halo at the neutron drip line in Zr and Ca isotopes [33, 36]. A systematical study on  ${}^{259}\text{Db}$  and its  $\alpha$ -daughter nuclei were also achieved [28]. In principle, only a calculation in a large multidimensional deformation space can definitively decide the appropriate ground-state shape. However, as the traditional

superheavy nuclei are expected to be spherical and are located on the nuclear chart around a spherical doubly magic nucleus next to  $^{208}_{126}\text{Pb}$  [37], the RCHB theory with the assumption of spherical shape can be applied to this preliminary scan for magic numbers. It is the aim of this paper to predict doubly magic superheavy nuclei within the RCHB theory using a variant of the RMF interactions. As most of the presently found superheavy nuclei have large deformations, we will study the potential energy surface with the deformed-constrained RMF theory in order to confirm that the spherical configuration exists in these doubly magic nuclei.

The material contained in this study is organized as follows. The framework of RCHB and constrained RMF theory are outlined in Section II. Section III contains the predictions made from the two-nucleon separation energies  $S_{2p}$  and  $S_{2n}$ , the two-nucleon gaps  $\delta_{2p}$  and  $\delta_{2n}$ , the shell correction energies  $E_{shell}^p$  and  $E_{shell}^n$ , the pairing energies  $E_{pair}^p$  and  $E_{pair}^n$ , and the pairing gap  $\Delta_p$  and  $\Delta_n$ , obtained in the RCHB theory with interactions NL1 [38], NL3 [39], NLSH [40], TM1 [41], TW99 [42], DD-ME1 [43], PK1 and PK1R [44]. The  $\alpha$ -decay half-lives are also discussed there. The binding energy and the corresponding macroscopic energy as a function of deformation obtained in the deformation-constrained RMF calculation for  $Z=120$  are presented in Sec. IV. Additionally, the formation cross sections for the possible doubly magic nuclei  $^{292}_{120}$  and  $^{304}_{120}$  at the optimal excitation energy are estimated by a phenomenological model proposed by Smolańczuk [45] with the input from the constrained RMF theory. Finally, Section V contains the main conclusions of this work.

## II. FRAMEWORK

### A. Relativistic continuum Hartree-Bogoliubov theory

The basic ansatz of the RMF theory is a Lagrangian density where nucleons are described as Dirac particles which interact via the exchange of various mesons. The Lagrangian density

considered has the form:

$$\begin{aligned}
\mathcal{L} = & \bar{\psi} \left[ i\gamma^\mu \partial_\mu - M - g_\sigma \sigma - g_\omega \gamma^\mu \omega_\mu - g_\rho \gamma^\mu \vec{\tau} \cdot \vec{\rho}_\mu - e\gamma^\mu \frac{1-\tau_3}{2} A_\mu \right] \psi \\
& + \frac{1}{2} \partial^\mu \sigma \partial_\mu \sigma - \frac{1}{2} m_\sigma^2 \sigma^2 - \frac{1}{3} g_2 \sigma^3 - \frac{1}{4} g_3 \sigma^4 \\
& - \frac{1}{4} \Omega^{\mu\nu} \Omega_{\mu\nu} + \frac{1}{2} m_\omega^2 \omega^\mu \omega_\mu + \frac{1}{4} c_3 (\omega^\mu \omega_\mu)^2 \\
& - \frac{1}{4} \vec{R}^{\mu\nu} \cdot \vec{R}_{\mu\nu} + \frac{1}{2} m_\rho^2 \vec{\rho}^\mu \cdot \vec{\rho}_\mu + \frac{1}{4} d_3 (\vec{\rho}^\mu \cdot \vec{\rho}_\mu)^2 \\
& - \frac{1}{4} F^{\mu\nu} F_{\mu\nu}
\end{aligned} \tag{1}$$

where  $\psi$  is Dirac spinor and  $\bar{\psi} = \psi^\dagger \gamma^0$ .  $M$ ,  $m_\sigma$ ,  $m_\omega$ , and  $m_\rho$  are the nucleon,  $\sigma$ ,  $\omega$  and  $\rho$  meson masses respectively, while  $g_\sigma$ ,  $g_2$ ,  $g_3$ ,  $g_\omega$ ,  $c_3$ ,  $g_\rho$ ,  $d_3$ , and  $e^2/4\pi = 1/137$  are the corresponding coupling constants for the mesons and the photon. The field tensors of the vector mesons ( $\omega$  and  $\rho$  mesons) and of the electromagnetic fields take the following form:

$$\begin{aligned}
\Omega^{\mu\nu} &= \partial^\mu \omega^\nu - \partial^\nu \omega^\mu \\
\vec{R}^{\mu\nu} &= \partial^\mu \vec{\rho}^\nu - \partial^\nu \vec{\rho}^\mu - 2g_\rho \vec{\rho}^\mu \times \vec{\rho}^\nu \\
F^{\mu\nu} &= \partial^\mu A^\nu - \partial^\nu A^\mu
\end{aligned} \tag{2}$$

With the classical variational principle, one can obtain the coupled equations of motion, which contain the Dirac equation for the nucleons and the Klein-Gordon type equations for the mesons and the photon. The coupled equations are self-consistently solved by iterations.

For the RMF theory, however, as the classical meson fields are used, the equations of motion for nucleons derived from Eq. (1) do not contain pairing interaction. In order to have two-body interaction, one has to quantize the meson fields which leads to a Hamiltonian with two-body interaction. Following the standard procedure of Bogoliubov transformation, a Dirac Hartree-Bogoliubov equation could be derived and then a unified description of the mean field and pairing correlation in nuclei could be achieved [46]. The Dirac Hartree-Bogoliubov equations are as following:

$$\int d^3r' \begin{pmatrix} h - \lambda & \Delta \\ \Delta & -h + \lambda \end{pmatrix} \begin{pmatrix} \psi_U \\ \psi_V \end{pmatrix} = E \begin{pmatrix} \psi_U \\ \psi_V \end{pmatrix}, \tag{3}$$

where,  $h = \vec{\alpha} \cdot \vec{p} + g_\omega \omega + g_\rho \tau_3 \rho + \beta(M + g_\sigma \sigma)$  is the Dirac Hamiltonian and the Fock term has been neglected as is usually done in RMF. A Lagrange multiplier  $\lambda$  is introduced to adjust

the proper particle number of neutrons and protons. The pairing potential  $\Delta$  in Eq. (3) is :

$$\Delta_{ab} = \frac{1}{2} \sum_{cd} V_{abcd}^{pp} \kappa_{cd}. \quad (4)$$

It is obtained from one-meson exchange interaction  $V_{abcd}$  in the  $pp$ -channel and the pairing tensor  $\kappa = \psi_U^* \psi_V^T$ . The interaction  $V_{abcd}$  used for the pairing potential in Eq. (4) is either the density-dependent two-body force of zero range or Gogny-type finite range force as shown in Ref. [31]. Considering the consuming computational time, we prefer to use the density-dependent zero range  $\delta$  force with the interaction strength  $V_0$  and the nuclear matter density  $\rho_0$  as

$$V(\vec{r}_1, \vec{r}_2) = V_0 \delta(\vec{r}_1 - \vec{r}_2) \frac{1}{4} [1 - \vec{\sigma}_1 \cdot \vec{\sigma}_2] \left( 1 - \frac{\rho(r)}{\rho_0} \right). \quad (5)$$

The relativistic continuum Hartree-Bogoliubov theory solves the RHB equations in the coordinate representation in order to describe both the continuum and the bound states self-consistently [31]. It is then applicable to not only stable nuclei but also exotic nuclei. When the  $\delta$ -force in the pairing channel is used, the RCHB equations are a set of four coupled differential equations, which are solved in a self-consistent way by the shooting method and the Runge-Kutta algorithm. More details can be found in Ref. [31].

In this paper, the RCHB equations are solved in a spherical box with radius  $R=25$  fm, the step size of 0.1 fm, and proper boundary conditions. It has been shown in Refs. [31, 33] that the results do not depend on the box size when  $R \geq 15$  fm. The strength  $V_0$  of the pairing force for proton and neutron is fixed at  $-650 \text{ MeV}\cdot\text{fm}^{-3}$ . For  $\rho_0$  we use the nuclear matter density  $0.152 \text{ fm}^{-3}$ .

## B. Deformation-constrained RMF theory

To examine the ground state geometrical configuration of certain heavy or superheavy nucleus, as well as its fission barrier, one has to obtain the potential energy surface. The potential energy curve can be calculated microscopically by the deformation-constrained RMF theory. The binding energy at certain deformation value is obtained by constraining the quadrupole moment  $\langle Q_2 \rangle$  to a given value  $\mu_2$  in the expectation value of the Hamiltonian [47],

$$\langle H' \rangle = \langle H \rangle + \frac{1}{2} C_\mu (\langle Q_2 \rangle - \mu_2)^2, \quad (6)$$

where  $C_\mu$  is the constraint multiplier. The expected value of the quadrupole moment operator is  $\langle Q_2 \rangle = \langle Q_2^n \rangle + \langle Q_2^p \rangle$ , where the quadrupole moment operator for neutrons (protons) is calculated by  $\langle Q_2^{n(p)} \rangle = \langle 2r^2 P_2(\cos \theta) \rangle_{n(p)}$ . The equations of motion are solved by expanding the Dirac spinors in harmonic oscillator basis in the cylindrical coordinates. The size of the basis is crucial and responsible for the reliability of the result. By varying  $\mu_2$ , the binding energy at different deformation can be obtained. The pairing is taken into account by the constant gap approximation (BCS) in which the pairing gap is taken as  $\frac{12}{\sqrt{A}}$  for even number nucleons. An enormous advantage of microscopic constrained RMF calculations compared with the phenomenological calculations is that in the microscopic constrained calculation we need only follow a one-parameter line, e.g.  $\beta_2$ , while in the phenomenological methods we must calculate multidimensional energy surfaces [47].

### III. MAGIC NUMBERS IN SUPERHEAVY NUCLEI

The doubly magic nuclei are searched for the even-even nuclei (more than 1200 nuclei) in the nuclear chart with proton number  $Z=100 - 140$  and neutron number  $N=(Z+30) - (2Z+32)$  (i.e.,  $N=130 - 312$ ) by the RCHB calculation with the effective interactions NL1 [38], NL3 [39], NLSH [40], TM1 [41], TW99 [42], DD-ME1 [43], PK1 and PK1R [44]. These nuclei are presented as shaded area in Fig. 1. The long-dashed line and solid line in Fig. 1 represent the  $\beta$ -stability line of the parametrization

$$N - Z = 6 \times 10^{-3} \cdot A^{5/3} \quad (7)$$

from Ref. [48] and

$$Z = \frac{A}{1.98 + 0.0155 \cdot A^{2/3}} \quad (8)$$

from Ref. [49], respectively. The black dots lying at the lower-left corner represent the superheavy nuclei which have been observed or declared to be observed experimentally [50]. The vertical and horizontal lines in Fig. 1 represent the possible magic proton and neutron numbers which will be discussed later.

For RMF calculations, there exist many effective interactions, which provide nearly equal quality of description for stable nuclei. However, when they are applied to the exotic nuclei, the differences appear. In view of the uncertainties, the effective interactions considered here are four frequently used interactions NL1, NL3, NLSH, TM1, density-dependent interactions

TW99 and DD-ME1, as well as the newly developed PK1 and PK1R which were adjusted with the elaborate consideration of the cent-of-mass correction. The effective interactions PK1 and PK1R are listed in Table I.

In the following four subsections, the signatures of shell closure on the two-nucleon separation energies  $S_{2p}$  and  $S_{2n}$ , the two-nucleon gaps  $\delta_{2p}$  and  $\delta_{2n}$ , the shell correction energies  $E_{shell}^p$  and  $E_{shell}^n$ , the pairing energies  $E_{pair}^p$  and  $E_{pair}^n$  and the pairing gaps  $\Delta_p$  and  $\Delta_n$  obtained in RCHB calculation will be analyzed consecutively. The  $\alpha$ -decay half-lives  $T_\alpha$  will be discussed afterwards. At last, the prediction of the magic proton and neutron numbers in superheavy nuclei will be summarized.

### A. Two-nucleon separation energies

The two-nucleon separation energy,

$$S_{2n}(N, Z) = E_B(N, Z) - E_B(N - 2, Z), \quad S_{2p}(N, Z) = E_B(N, Z) - E_B(N, Z - 2) \quad (9)$$

is better to quantify shell effects than the single-nucleon separation energy due to the absence of odd-even effects, here  $E_B(N, Z)$  is the binding energy of the nucleus  ${}^{N+Z}\text{Z}$ . For an isotonic chain, the  $S_{2p}$  become smaller with the proton number  $Z$ . A jump of  $S_{2p}$  indicates the occurrence of a proton shell closure.

For the sake of a clear presentation of the results, the two-proton separation energies  $S_{2p}$  from the RCHB calculation for even-even nuclei with  $Z=102 - 140$  as a function of mass number  $A$  with the effective interactions NL1, NL3, NLSH, TM1, TW99, DD-ME1, PK1, and PK1R are shown in Fig. 2. In the figure,  $S_{2p}(N, Z)$  for the same  $Z$  are connected to form a curve so that the jumps of  $S_{2p}$  compose a gap between the curves. The 20  $S_{2p}$  curves in each subfigure correspond to isotopic chains for  $Z$  ranging from 102 to 140 with a step of two. The curve at the upper-left corner is for  $Z=102$  and the neighboring one is for  $Z=104$ , and so on.

For an isotonic chain, the  $S_{2p}$  gradually decrease from about 25 MeV to zero for the curve at the upper-left corner to the lower-right corner. Each curve is roughly in parallel with the other. A gap is enchased if a magic proton number exists. Take  $S_{2p}$  for the effective interaction NL1 as an example: the gap between  $Z=120$  and  $Z=122$  (abbr. at  $Z=120$ ) is large and stable, the gap at  $Z=132$  is visible just in the region  $N=220 - 250$ , and the gap



at  $Z=138$  is relatively large but unstable. The gap at  $Z=138$  becomes weak at  $N \approx 240$ .

For all effective interactions, the magic proton numbers  $Z=120, 132,$  and  $138$  are common while  $Z=106$  is observed only for NL3, NLSH, TW99, PK1, and PK1R. Generally, the gaps do not exist for all isotopes, e.g., the gap at  $Z=132$  for NL1 exists only for  $N=220 - 250$ , and the gap at  $Z=138$  for PK1 exists only for  $N=230 - 270$ .

Fig. 3 is the same as Fig. 2, but for  $S_{2n}$  with  $N=132 - 312$ . Each curve corresponds to an isotonic chain. The upper-left curve is for  $N=132$  and the difference of the neutron number between the neighboring curves is 2.

The gaps of  $S_{2n}$  are more complicated than those of  $S_{2p}$ . For fixed  $Z$ ,  $S_{2n}$  decrease gradually with  $N$ . For effective interaction NL1, there are nine gaps at  $N=138, 172, 184, 198, 228, 238, 252, 258,$  and  $274$ . The size and the shape of the gaps differ notably: The gaps at  $N=172, 184,$  and  $258$  are relatively larger than the other gaps.

For all effective interactions,  $S_{2n}$  show distinguishable gaps at  $N=138, 172, 184, 198, 228, 238, 252, 258,$  and  $274$ . Such gaps mark the magic neutron number. Apart from the above mentioned common gaps, there are also other gaps which appear only for some effective interactions, i.e.,  $N=164$  for NLSH, TW99, DD-ME1, PK1 and PK1R, and  $N=216$  for NLSH, TW99, PK1, and PK1R. For the magic numbers marked either by the common gaps or the interaction-dependent gaps, the shell quenching phenomena, i.e., the gaps at  $N=184, 198$  (NL1),  $216$ (NLSH, TW99, PK1, and PK1R),  $228$  (NL1, NL3, NLSH, TM1, PK1, and PK1R),  $238, 252,$  and  $258$  (NLSH, TM1, PK1, and PK1R) appear only for certain  $Z$ , are observed.

Summarizing the above results, we may say that based on two-nucleon separation energies  $S_{2p}$  and  $S_{2n}$ ,  $Z=120, 132,$  and  $138$  ,and  $N=138, 172, 184, 198, 228, 238, 252, 258,$  and  $274$ , are the magic numbers predicted in the RCHB calculation. They are independent of the effective interactions used in the calculation. There are also some other magic numbers, e.g.,  $Z= 106$  and  $N= 164$  and  $216$ , which appear only for some effective interactions.

## B. Two-nucleon gaps

The changes of the two-nucleon separation energies can also be quantified by the second difference of the binding energies, i.e., the two-nucleon gaps:

$$\delta_{2n}(N, Z) = 2E_B(N, Z) - E_B(N + 2, Z) - E_B(N - 2, Z) = S_{2n}(N, Z) - S_{2n}(N + 2, Z) - S_{2n}(N - 2, Z)$$

$$\delta_{2p}(N, Z) = 2E_B(N, Z) - E_B(N, Z + 2) - E_B(N, Z - 2) = S_{2p}(N, Z) - S_{2p}(N, Z + 2) - S_{2p}(N, Z - 2)$$

A peak of the two-nucleon gap implicates the drastic changes of the two-nucleon separation energies, which can be used as the evidence of the magic number existence.

The two-proton gaps  $\delta_{2p}$  from the RCHB calculation for even-even nuclei with  $Z=102$  - 138 as a function of  $Z$  with the above eight effective interactions are shown in Fig. 4. The two-proton gaps  $\delta_{2p}$  with the same  $N$  are connected as a curve. A peak at certain  $Z$  in the curve suggests the existence of magic proton number. The sharpness of the peaks represent the goodness of the magic numbers while the quenching effects are associated with the bundle of the curves at the certain  $Z$ . The size of the gaps of two-proton separation energies  $S_{2p}$  in Fig. 2 correspond to the magnitude of the peaks of two-proton gaps  $\delta_{2p}$  in Fig. 4. Generally the magic numbers indicated by two-proton separation energies  $S_{2p}$  are supported by two-proton gaps  $\delta_{2p}$ . It is observed that common magic proton numbers  $Z=120, 132,$  and  $138$  exist for all effective interactions while  $Z=106$  is observed only for NL3, NLSH, TW99, DD-ME1, PK1, and PK1R. Furthermore, the peak at  $Z=114$  for NLSH and TW99 and the peak at  $Z=126$  for NL1 are also observed, though they are not so obvious as that at  $Z=120$ .

As counterpart of two-proton gaps  $\delta_{2p}$ , two-neutron gaps  $\delta_{2n}$  from the RCHB calculation for even-even nuclei  $N=132$  - 308 with effective interactions NL1, NL3, NLSH, TM1, TW99, DD-ME1, PK1, and PK1R are shown in Fig. 5. There are interaction-independent peaks of two-neutron gaps  $\delta_{2n}$  at  $N=138, 172, 184, 198, 228, 238, 258,$  and  $274$  which are consistent with the common gaps of two-neutron separation energies  $S_{2n}$  in Fig. 3. Moreover, small peaks are also observed for  $N=154$  (NLSH and TW99),  $N=164$  (NL3, NLSH, TW99, DD-ME1, PK1, and PK1R), and  $N=216$  (NLSH, TW99, PK1, and PK1R).

In general, based on two-nucleon gaps  $\delta_{2p}$  and  $\delta_{2n}$ , the magic numbers  $Z=120, 132,$  and  $138,$  and  $N=138, 172, 184, 198, 228, 238, 258,$  and  $274$  can also be observed for RCHB calculation with all effective interactions. Apart from  $Z=106$  and  $N=164$  and  $216,$  additional

magic numbers  $Z=114$  and  $126$ ,  $N=154$  appear in the two-nucleon gaps  $\delta_{2p}$  and  $\delta_{2n}$  in Figs. 4 and 5 for some effective interactions.

### C. Shell correction energies

The shell correction energy, representing the overall behavior of the single-particle spectra, may be a good candidate to identify the magicity. This quantity, which is derived from the single-particle spectra, is defined as the difference between the total single-particle energy  $E$  and the smooth single-particle energy  $\bar{E}$ :

$$E_{shell} = E - \bar{E} = \sum_{i=1}^{N(Z)} e_i - 2 \int_{-\infty}^{\bar{\lambda}} e \bar{g}(e) de. \quad (12)$$

where  $N(Z)$  is the particle number,  $e_i$  is the single-particle energy,  $\bar{\lambda}$  is the smoothed Fermi level and  $\bar{g}(e)$  is the smoothed level density. The shell correction energy provides an indicator about the deviation in the level structure of nuclei away from uniformly distributed ones. A large negative shell correction energy corresponds to shell closure at particular nucleon number.

The shell correction energy can be obtained by the Strutinsky procedure, in which the smoothed Fermi level  $\bar{\lambda}$  is determined by the particle number equation  $N(Z) = 2 \int_{-\infty}^{\bar{\lambda}} \bar{g}(e) de$ . The smoothed level density  $\bar{g}(e)$  takes the form:

$$\bar{g}(e) = \frac{1}{\gamma} \int_{-\infty}^{\infty} \left( \sum_{i=1}^{\infty} \delta(e' - e_i) \right) f\left(\frac{e' - e}{\gamma}\right) de' = \frac{1}{\gamma} \sum_{i=1}^{\infty} f\left(\frac{e_i - e}{\gamma}\right). \quad (13)$$

where  $\gamma$  is the smoothing range, the folding function  $f(x) = \frac{1}{\sqrt{\pi}} e^{-x^2} P(x)$ , and  $P(x)$  is an associated Laguerre polynomial  $L_s^{1/2}(x^2)$ .

In present calculation, the smoothing range is  $\gamma = 1.2$  and the order of the associated Laguerre polynomial is  $s = 3$ . The unit of  $\gamma$  is  $41 A^{-1/3} \left(1 \pm \frac{1}{3} \frac{N - Z}{A}\right)$  MeV where the plus (minus) sign holds for neutrons (protons). Then the particle number equation can be evaluated as:

$$N(Z) = 2 \sum_{i=1}^{\infty} \left[ \frac{1 - \text{erf}(t_i)}{2} - \frac{e^{-t_i^2}}{48\sqrt{\pi}} (57t_i - 32t_i^3 + 4t_i^5) \right], \quad (14)$$

where  $t_i = \frac{e_i - \bar{\lambda}}{\gamma}$  and  $\text{erf}(t_i)$  is the error function. The corresponding smooth single-particle energy  $\bar{E}$  takes the form:

$$\bar{E} = 2 \sum_{i=1}^{\infty} \left\{ e_i \left[ \frac{1 - \text{erf}(t_i)}{2} - \frac{e^{-t_i^2}}{48\sqrt{\pi}} (57t_i - 32t_i^3 + 4t_i^5) \right] - \gamma \frac{e^{-t_i^2}}{96\sqrt{\pi}} (15 - 90t_i^2 + 60t_i^4 - 8t_i^6) \right\}. \quad (15)$$

With the proton single-particle spectra in canonical basis from the RCHB calculation for even-even nuclei with  $Z=100 - 140$  as a function of  $Z$  with effective interactions NL1, NL3, NLSH, TM1, TW99, DD-ME1, PK1, and PK1R, the shell correction energies for proton  $E_{shell}^p$  are shown in Fig. 6. The nuclei with the same  $N$  are connected as a curve. A deep valley at certain  $Z$  on a curve hints the magicity. The valleys at  $Z=120, 132,$  and  $138$  are conspicuous for all effective interactions. Possible shell closure at  $Z=106$  for NL1, NL3, NLSH, TW99, DD-ME1, PK1, and PK1R, at  $Z=114$  for NLSH, TW99, PK1, and PK1R, and at  $Z=126$  for NL1 are also observed. The shell closure from the shell correction energies for proton  $E_{shell}^p$  in Fig. 6 are consistent with the peaks of the two-proton gaps  $\delta_{2p}$  in Fig. 4, though the magnitude of magicity slightly differs. Similar to two-proton gaps  $\delta_{2p}$ , the spread of the valleys of the shell correction energies for proton  $E_{shell}^p$  indicates the quenching of the magic number. In view of the shell correction energies for proton  $E_{shell}^p$ , the quenching phenomena of magic proton numbers in RCHB calculation are universal. These facts suggest that the magic proton numbers depend also on neutron number  $N$ .

The corresponding shell correction energies for neutron  $E_{shell}^n$  from the RCHB calculation for even-even nuclei with  $N=130 - 312$  as a function of  $N$  are demonstrated in Fig. 7. As the neutron numbers extends from  $N=130$  to  $N=290$ , the valleys for shell correction energies for neutron  $E_{shell}^n$  in Fig. 7 are not so obvious as those for shell correction energies for proton  $E_{shell}^p$  in Fig. 6. However, similar conclusions as two-neutron separation energies  $S_{2n}$  in Fig. 3 and two-neutron gaps  $\delta_{2n}$  in Fig. 5 for magic neutron numbers can also be drawn. For all effective interactions,  $N=184$  and  $258$  are found to be the common magic numbers. Similar calculation has also be done in Ref. [51] with SHF and RMF. From the shell correction energies for neutron, although the magic neutron numbers are not so sharp as those got from two-neutron separation energies  $S_{2n}$  and two-neutron gaps  $\delta_{2n}$ , however, the small irregularity in the shell correction energies still correspond to the magic number discussed above.

The first valley locates in  $N=184$  for all effective interactions and involves with  $N=172$

(NL3, NLSH, TM1, TW99, DD-ME1, PK1, and PK1R), even with  $N=164$  (NLSH and TW99). And the other valley is the mixture of the valleys at  $N=228$  (TW99 and DD-ME1),  $N=252$  (NLSH, TM1, PK1, and PK1R) and  $N=258$ . These fine structures suggest the smearing of magic neutron numbers.

Summarizing the above results, we may say that based on shell correction energies, the shell closures are smeared than those for two-nucleon separation energies  $S_{2p}$  and  $S_{2n}$  and two-nucleon gaps  $\delta_{2p}$  and  $\delta_{2n}$ , however we can observe magic numbers at  $Z=120, 132,$  and  $138$  are common and strongly quenched, the shell closures near  $N=172$  and  $N=184,$  and  $N=228, N=252,$  and  $N=258$  are blurred. The other magic numbers from the shell correction energies, such as  $Z=106, 114,$  and  $126,$  appear only for some effective interactions.

#### D. Pairing energies and pairing gaps

In this subsection we will investigate the pairing effects, which can also provide reliable information of nuclear magic number, including the pairing energy and the effective pairing gap. The pairing energy in RHB theory is given by

$$E_{pair} = -\frac{1}{2}\text{Tr}\Delta\kappa, \quad (16)$$

where  $\Delta$  and  $\kappa$  are the pairing potential and the pairing tensor respectively. Generally speaking the pairing energies vanish at the closed shell and have a maximum values in the middle of two closed shells. Similarly, the effective pairing gap defined as

$$\Delta_{n(p)} = \frac{\sum_i \Delta_i v_i^2 (2j+1)}{N(Z)}, \quad (17)$$

can also be used to denote the shell closure, where the sum  $i$  is over the single particle levels of neutron or proton in the canonical basis[31],  $2j+1$  is the degeneracy number of the corresponding energy level  $i$  and  $N(Z)$  is the particle number,  $\Delta_i$  is the pairing gap for level  $i$  in canonical basis determined by  $(E_i - \lambda) \cdot 2u_i v_i = \Delta_i (v_i^2 - u_i^2)$  where  $\lambda$  is the Fermi energy and the particle and hole amplitude  $u_i, v_i$  satisfies  $u_i^2 + v_i^2 = 1$ .

The pairing energies for proton  $E_{pair}^p$  and the effective pairing gaps for proton  $\Delta_p$  from the RCHB calculation for even-even nuclei with  $Z=100 - 140$  as a function of  $Z$  with effective interactions NL1, NL3, NLSH, TM1, TW99, DD-ME1, PK1, and PK1R are shown in Figs. 8 and 9 respectively. Both figures has the same pattern while the shell closures in Fig. 9 are

more clear. It is observed that common magic proton numbers  $Z=120$ ,  $132$ , and  $138$  exist for all effective interactions while  $Z=106$  exists only for NL1, NL3, NLSH, TW99, DD-ME1, PK1, and PK1R,  $Z=114$  exists only for NL3, NLSH, TW99, DD-ME1, PK1, and PK1R, and  $Z=126$  exists only for NL1, TW99, DD-ME1. Generally the shell closures are quenched for all magic proton numbers. It should be noted that the peak at  $Z=120$  for NL1, TW99, and DD-ME1 is stable for all isotopes while for NLSH, TM1, PK1, and PK1R, it is quenched.

Fig. 10 shows the pairing energies for neutron  $E_{pair}^n$  from the RCHB calculation for even-even nuclei with  $N=130 - 312$  as a function of  $N$  with eight effective interactions. The vanishing of pairing at  $N=138$ ,  $164$ ,  $172$ ,  $184$ ,  $198$ ,  $228$ ,  $238$ ,  $252$ ,  $258$ , and  $274$  are common for all interactions while the vanishing of pairing at  $N=154$  and  $N=216$  exist only for NL3, NLSH, TW99, PK1, and PK1R, and while the vanishing of pairing at  $N=210$  exists only for DD-ME1. The same pattern is observed by the effective pairing gaps for neutron  $\Delta_n$  in Fig. 11.

From the above discussion, the magic numbers  $Z=120$ ,  $132$ , and  $138$  and  $N=138$ ,  $164$ ,  $172$ ,  $184$ ,  $198$ ,  $228$ ,  $238$ ,  $252$ ,  $258$ , and  $274$  are supported by the pairing energies and the effective pairing gaps.

### E. Alpha decay half-lives

Alpha decay is one of the most predominant decay modes for superheavy nuclei. For an area of enhanced stability, the  $\alpha$ -decay half-lives are expected to be longer than its neighbors. The phenomenological formula of Viola and Seaborg [52] for calculation of  $\alpha$ -decay half-lives with the parameter in Ref. [7]:

$$\log_{10}T_{\alpha} = (1.66175Z_P - 8.5166)Q_{\alpha}^{-1/2} - (0.20228Z_P + 33.9069) \quad (18)$$

are used, where  $Z_P$  is the proton number of a parent nucleus,  $Q_{\alpha}$  is the  $\alpha$ -decay energy  $Q_{\alpha} = E_B(Z - 2, N - 2) - E_B(Z, N) + 28.295673$  in MeV, and  $T_{\alpha}$  is in seconds. It should be noted that Eq.(18) is based on the WKB approximation, and provides only a rather crude estimate of  $T_{\alpha}$  since it disregards many structure effects such as deformation, and configuration changes, etc.

In Fig. 12, we plot the half-lives  $T_{\alpha}$  from the RCHB calculation in logarithm scale as a function of neutron number  $N$  with effective interactions NL1, NL3, NLSH, TM1, TW99,

DD-ME1, PK1 and PK1R. The half-lives correspond to 1ns, 1 $\mu$ s, 1ms, 1s, 1h, 1y, and 1ky are marked by the dashed lines. Each curve in this figure corresponds to an isotopic chain in the region  $Z=102-140$ . In Fig. 12, the half-lives  $\log_{10}T_\alpha$  increase with  $N$ . The jumps of the curves correspond to magic proton numbers  $Z=106, 120, 132,$  and  $138$ , which depend on the effective interactions. The peaks of each curve correspond to magic neutron numbers, i.e.,  $N=172, 184, 228, 238$  and  $258$ . It can be seen that the magic numbers suggested by two-neutron separation energies  $S_{2n}$ (two-neutron gaps  $\delta_{2n}$ ) or two-proton separation energies  $S_{2p}$ (two-proton gaps  $\delta_{2p}$ ) can also be found here.

So far, the RCHB theory with eight different interactions, namely NL1, NL3, NLSH, TM1, TW99, DD-ME1, PK1 and PK1R has been applied to the superheavy region with proton number  $Z=100 - 140$  and neutron number  $N= (Z+30) - (2Z+32)$ . After detailed analyses on two-nucleon separation energies  $S_{2p}$  and  $S_{2n}$ , two-nucleon gaps  $\delta_{2p}$  and  $\delta_{2n}$ , the shell correction energies  $E_{shell}^p$  and  $E_{shell}^n$ , as well as the pairing energies  $E_{pair}^p$  and  $E_{pair}^n$ , the effective pairing gaps  $\Delta_p$  and  $\Delta_n$ , the magic numbers are predicted. Table II and Table III list the possible magic proton and neutron numbers suggested by the above quantities and interactions. In these tables, the physical quantity (row-wise) corresponding to the magicity of certain proton number (column-wise) is marked as a black square for each interaction. According to Table II and Table III, the doubly magic superheavy nuclei can be the combination of magic proton numbers  $Z=120, 132,$  and  $138$  and magic neutron numbers  $N=172, 184, 198, 228, 238,$  and  $258$ . Such magic numbers are presented as gray lines in Fig. 1. It should be noted that the crosses of lines in Fig. 1 do not necessary mean doubly magic nuclei as there are also shell quenching effects. However, these crosses include all the possible doubly magic nuclei in the state-of-the-art relativistic approach.

#### IV. DOUBLY MAGIC NUCLEI IN SUPERHEAVY NUCLEI

The magic numbers obtained before with the RCHB theory are based on the assumption of spherical geometrical configuration. However, the assumption is not always true for superheavy nuclei. In fact, most superheavy nuclei found experimentally are known to be deformed. It is worthy to investigate the potential energy surfaces in order to see the validity of spherical configuration. For this purpose, the deformation-constrained RMF

calculations have been done. The deformation parameter  $\beta_2$  of the harmonic oscillator basis (with 20 shells) is set to the expected deformation to obtain high accuracy and reduce the computing times. Although such calculation is very lengthy for superheavy nuclei, we have systematically calculated the potential energy surfaces for all the possible doubly magic nuclei with the effective interaction NL3. The calculation with other interactions for some typical doubly magic nuclei are also done for comparison. To save space, only the results for  $Z=120$  isotopes with NL3 are presented here.

In Fig. 13, the potential energy surfaces for nuclei  $^{292}120$ ,  $^{304}120$ ,  $^{318}120$ ,  $^{348}120$ ,  $^{358}120$ , and  $^{378}120$  are presented with the solid lines in corresponding subfigures. These nuclei are clearly shown as the crosses with  $Z = 120$  in Fig. 1. Although these nuclei have the same proton number, their potential energy surfaces are quite different from each other. For nuclei  $^{292}120$ ,  $^{304}120$  and  $^{378}120$ , there is an obvious local minimum with the spherical configuration  $\beta_2 \sim 0$ , while another local minimum with large deformation  $\beta_2 \sim 0.6$  can be also clearly seen. For  $^{318}120$ , the spherical local minimum is very shallow, and for  $^{348}120$  and  $^{358}120$ , the spherical minimum is hardly seen and a local minimum with  $\beta_2 \sim 0.25$  appears instead. In addition to the local minima discussed, we should make remark on the absolute minima for these nuclei. For  $^{292}120$  and  $^{378}120$ , the two minima with the different deformation are almost with the same energies, i.e. the so-called “shape coexistence”, may exist. In particular, the spherical minimum is indeed the absolute minimum for  $^{292}120$  ( $E_B = -2064.3$  MeV with  $\beta_2 \sim 0$  vs.  $E_B = -2063.2$  MeV with  $\beta_2 \sim 0.6$ ), while the ground state of  $^{378}120$  is quite delicate with  $E_B = -2398.7$  MeV for  $\beta_2 \sim 0$  and  $E_B = -2398.9$  MeV for  $\beta_2 \sim 0.6$ . For  $^{304}120$ , the absolute minimum at  $\beta_2 \sim 0.6$  is much deeper ( $\sim 6.1$  MeV) than the spherical configuration. In addition for  $^{348}120$ , the absolute minimum lies at  $\beta_2 \sim 0.2$ , and it is a well-deformed nucleus according to the present calculation.

To investigate the role of shell effects for superheavy nuclei, the corresponding macroscopic energies as a function of deformation  $\beta_2$  with the effective interaction NL3 are presented as the dashed lines in Fig. 13. The macroscopic energy is defined as the difference between the binding energy and the total shell correction energy which is obtained similarly as in Section III.C. It can be seen that without the shell effects, the superheavy nuclei hardly exist. It is the shell effects that play an essential role to stabilize the superheavy nuclei against the fission. In Fig. 14, the shell correction energies for neutrons, protons, and nucleons are respectively presented as the dot-dashed, dashed lines, and solid lines.



With the same proton number  $Z=120$ , the shell correction energies  $E_{shell}$  in these nuclei sensitively depends on the deformation  $\beta_2$ . The shell correction energies for protons  $E_{shell}^p$  at  $\beta_2 = 0$  are respective  $-5.5$ ,  $-4.0$ ,  $-1.6$ ,  $-0.7$ ,  $-1.1$ , and  $-1.8$  MeV for  $^{292}120$ ,  $^{304}120$ ,  $^{318}120$ ,  $^{348}120$ ,  $^{358}120$ , and  $^{378}120$ , which partly explain the spherical configuration in Fig. 13. In contrast to  $E_{shell}^p$ , the shell correction energies for neutrons  $E_{shell}^n$  at  $\beta_2 = 0$  are respective  $-6.1$ ,  $-2.6$ ,  $2.1$ ,  $-0.4$ ,  $-5.5$ , and  $-13.5$  MeV. Due to the large  $E_{shell}^p$  and / or  $E_{shell}^n$  energies, the outstanding spherical local minima for  $^{292}120$ ,  $^{304}120$  and  $^{378}120$  are seen in Fig. 13. From the constrained RMF calculation, we can conclude that for the  $Z = 120$  isotope chain,  $^{292}120$  and  $^{378}120$  would be doubly magic nuclei with spherical configuration.

Inspiring by the spherical absolute minimum of  $^{292}120$  calculated by constrained RMF theory with NL3, we use the simple cold fusion model with the doubly magic nuclei  $^{208}\text{Pb}$  as a target to estimate the formation cross section  $\sigma$  for  $^{292}120$  and  $^{304}120$ , although it is noticed that the deformed actinide nuclei are recommended to synthesize superheavy nuclei with  $A > 112$  [53]. The properties of the nuclei including the microscopic energy extracted from the constrained RMF calculation are applied in the phenomenological model [45] with the reference reaction chosen as  $^{208}\text{Pb}(^{48}\text{Ca},1n)^{255}\text{No}$ . The free parameter  $C$  in the model is determined by assuming the formation cross section  $\sigma$  of the reference reaction, i.e.,  $\sigma(C_1)=500\text{nb}$  and  $\sigma(C_2)=260\text{nb}$ . In Table IV, the  $Q$  value, the height of the static fission barrier  $B_f^{stat}(\text{ER})$ , the optimal excitation energy  $E_{opt}^*$ , and the formation cross section  $\sigma$  at  $E_{opt}^*$  with the input from the constrained RMF for effective interactions NL1, NL3, NLSH, and TM1 are listed. The strong dependence of the cross section  $\sigma$  on the RMF effective interactions can be seen. The largest cross section  $\sigma$  is given by NL1. Considered that the experimental measure limit of cross section  $\sigma$  is above 1pb, the two possible doubly magic nuclei  $^{292}120$  and  $^{304}120$  can be synthesized in the laboratory with the view for NL1. However the results from NL1 are not supported by the other RMF interactions. It should be mentioned that the results of NL3 are a little different from those of NLSH and TM1, it gives nearly accessible cross section ( $\sigma \sim 1$  pb) for  $^{292}120$ .

## V. SUMMARY

We have investigated the possible doubly magic nuclei in the superheavy region with proton number  $Z=100 - 140$  and neutron number  $N = (Z+30) - (2Z+32)$  within the RCHB

theory with interactions NL1, NL3, NLSH, TM1, TW99, DD-ME1, PK1, and PK1R. Shell closure are quantified in terms of the two-nucleon separation energies  $S_{2p}$  and  $S_{2n}$ , the two-nucleon gaps  $\delta_{2p}$  and  $\delta_{2n}$ , the shell correction energies  $E_{shell}^p$  and  $E_{shell}^n$ , the pairing energies  $E_{pair}^p$  and  $E_{pair}^n$  and the pairing gaps  $\Delta_p$  and  $\Delta_n$  obtained in the RCHB theory. The  $\alpha$ -decay half-lives are also discussed.  $Z=120$ , 132, and 138 and  $N=172$ , 184, 198, 228, 238, and 258 are inferred to be magic numbers. In addition, the spherical configuration of the doubly magic nuclei  $^{292}120$  is supported by examining the potential energy surfaces in the deformation-constrained RMF theory and is consistent with other studies applying relativistic forces[25]. The shell effects stabilizing the superheavy nuclei are emphasized by extracting the shell correction energies from the deformation-constrained RMF calculation. Finally the formation cross sections of  $^{292}120$  and  $^{304}120$  with  $^{208}\text{Pb}$  as a target are estimated. With the view of effective interaction NL1,  $^{292}_{172}120$  may be synthesized in the current experimental setup.

### Acknowledgments

This work is partly supported by the Major State Basic Research Development Program Under Contract Number G2000077407, the National Natural Science Foundation of China under Grant Nos. 10025522, and 10221003, and the Doctoral Program Foundation from the Ministry of Education in China.

- 
- [1] W. D. Myers and W. J. Swiatecki, Nucl. Phys. **A81**, 1 (1966).
  - [2] H. Meldner, Ark. Fys. **36**, 593 (1967).
  - [3] S. G. Nilsson, C. F. Tsang, A. Sobiczewski, Z. Szymański, S. Wycech, C. Gustafson, I.-L. Lamm, P. Möller, and B. Nilsson, Nucl. Phys. **A131**, 1 (1969).
  - [4] U. Mosel and W. Greiner, Z. Phys. **222**, 261 (1969).
  - [5] P. Möller, J. R. Nix, W. D. Myers, and W. J. Swiatecki, At. Data Nucl. Data Tables **59**, 185 (1995).
  - [6] S. Čwiok, V. V. Pashkevich, J. Dudek, and W. Nazarewicz, Nucl. Phys. **A410**, 254 (1983).
  - [7] A. Sobiczewski, Z. Patyk, and S. Čwiok, Phys. Lett. B **224** 1 (1989).

- [8] Z. Patyk and A. Sobiczewski, Nucl. Phys. **A533**, 132 (1991).
- [9] S. Hofmann, *et al.*, Z. Phys. A **350**, 277 (1995).
- [10] S. Hofmann, *et al.*, Z. Phys. A **350**, 281 (1995).
- [11] S. Hofmann, *et al.*, Z. Phys. A **354**, 229 (1996).
- [12] A. Ghiorso, *et al.*, Phys. Rev. C **51**, R2293 (1995).
- [13] Yu. A. Lazarev, *et al.*, Phys. Rev. Lett. **73**, 624 (1994).
- [14] Yu. A. Lazarev, *et al.*, Phys. Rev. Lett. **75**, 1903 (1995).
- [15] Yu. A. Lazarev, *et al.*, Phys. Rev. C **54**, 620 (1996).
- [16] Yu. Ts. Oganessian, *et al.*, Phys. Rev. Lett. **83**, 3154 (1999).
- [17] Yu. Ts. Oganessian, *et al.*, Phys. Rev. C **62**, 041604(R)(2000).
- [18] Yu. Ts. Oganessian, *et al.*, Phys. Rev. C **63**, 011301(R)(2000).
- [19] Yu. Ts. Oganessian, *et al.*, Phys. Rev. C **69**, 021601(R)(2004).
- [20] P. Möller and J. R. Nix, J. Phys. G **20**, 1681 (1994).
- [21] A. Sobiczewski, Sov. J. Part. Nucl. **25**, 119 (1994).
- [22] C. L. Wu, M. Guidry, and D. H. Feng, Phys. Lett. B **387**, 449 (1996).
- [23] G. A. Lalazissis, M. M. Sharma, P. Ring, and Y. K. Gambhir, Nucl. Phys. **A608**, 202 (1996).
- [24] S. Ćwiok, J. Dobaczewski, P.-H. Heenen, P. Magierski, and W. Nazarewicz, Nucl. Phys. **A611**, 211 (1996).
- [25] K. Rutz, M. Bender, T. Bürvenich, T. Schilling, P.-G. Reinhard, J. A. Maruhn, and W. Greiner, Phys. Rev. C **56**, 238 (1997).
- [26] M. Bender, K. Rutz, P.-G. Reinhard, J. A. Maruhn, and W. Greiner, Phys. Rev. C **60**, 034304 (1999).
- [27] J. Meng and N. Takigawa, Phys. Rev. C **61**, 064319 (2000).
- [28] W. Long, J. Meng, and S.-G. Zhou, Phys. Rev. C **65**, 047306 (2002).
- [29] L. S. Geng, H. Toki, and J. Meng, Phys. Rev. C **68**, 061303(R)(2003).
- [30] P. Ring, Prog. Part. Nucl. Phys. **37** 193 (1996)
- [31] J. Meng, Nucl. Phys. **A635**, 3 (1998).
- [32] J. Meng and P. Ring, Phys. Rev. Lett. **77**, 3963 (1996).
- [33] J. Meng and P. Ring, Phys. Rev. Lett. **80**, 460 (1998).
- [34] J. Meng, I. Tanihata, and S. Yamaji, Phys. Lett. B **419** 1 (1998).
- [35] J. Meng, S.-G. Zhou, and I. Tanihata, Phys. Lett. B **532**, 209 (2002)

- [36] J. Meng, H. Toki, J. Y. Zeng, S. Q. Zhang, and S.-G. Zhou, Phys. Rev. C **65**, 041302(R)(2002).
- [37] R. Smolańczuk, Phys. Rev. C **56**, 812 (1997).
- [38] Suk-Joon Lee, J. Fink, A. B. Balantekin, M. R. Strayer, A. S. Umar, P. -G. Reinhard, J. A. Maruhn, and W. Greiner, Phys. Rev. Lett. **57**, 2916 (1986).
- [39] G. A. Lalazissis, J. König, and P. Ring., Phys. Rev. C **55**, 540 (1997).
- [40] M. M. Sharma and P. Ring, Phys. Rev. C **45**, 2514 (1992).
- [41] Y. Sugahara and H. Toki, Nucl. Phys. **A579**, 557 (1994).
- [42] S. Typel and H. H. Wolter., Nucl. Phys. **A656**, 331 (1999).
- [43] T. Nikšić, D. Vretenar, P. Finelli, and P. Ring., Phys. Rev. C, **66**, 024306 (2002).
- [44] W. Long, J. Meng, N. V. Giai, and S.-G. Zhou, nucl-th/0311031, to be published in Phys. Rev. C.
- [45] R. Smolańczuk, Phys. Rev. C **59**, 2634 (1999).
- [46] H. Kucharek and P. Ring, Z. Phys. A **339**, 23 (1991).
- [47] P. Ring and P. Schuck, *The Nuclear Many-body Problem* 269 (Springer-Verlag, New York, 1980)
- [48] A. Bohr and B. R. Mottelson, *Nuclear Structure* Vol. 1 (W. A. Benjamin Inc. , New York, Amesterdam, 1969).
- [49] P. Marmier and E. Sheldon, *Physics of Nuclei and Particles* vol I. (Academic, New York and London, 1971).
- [50] Editorial Board of Nucl. Phys. Rev., *Nucl. Phys. Rev.* vol. Nuclear Chart (Science Press, Lanzhou, 2003).
- [51] M. Bender , W. Nazarewicz, and P.-G. Reinhard, Phys. Lett. B. **515**, 42 (2001).
- [52] V. E. Viola Jr. and G. T. Seaborg, J. Inorg. Nucl. Chem. **28** , 741 (1966).
- [53] P. Armbruster, C. R. Physique **4**, 571 (2003).

TABLE I: The effective interactions PK1 and PK1R[44]. The mass of the isovector vector meson is taken as  $m_\rho=763$  MeV for PK1 and PK1R.

Effective interactions	$m_\sigma$ [MeV]	$m_\omega$ [MeV]	$g_\sigma$	$g_\omega$	$g_\rho$ [fm <sup>-1</sup> ]	$g_2$	$g_3$	$c_3$	$d_3$
PK1	514.089	784.254	10.322	13.013	4.530	-8.169	-9.998	55.636	0
PK1R	514.087	784.222	10.322	13.013	4.550	-8.156	-10.198	54.446	350

TABLE II: The possible magic proton number suggested by two-proton separation energies, two-proton gaps, shell correction energies, pairing energies and effective pairing gaps for proton with interactions NL1, NL3, NL-SH, TM1, TW-99, DD-ME1, PK1 and PK1R, respectively.

Effective interactions	Quantity	Magic proton number candidates					
		106	114	120	126	132	138
NL1	$S_{2p}$			■		■	■
	$\delta_{2p}$			■	■	■	■
	$E_{shell}^p$	■		■	■	■	■
	$E_{pair}^p$	■		■	■	■	■
	$\Delta_p$	■		■	■	■	■
NL3	$S_{2p}$	■		■		■	■
	$\delta_{2p}$	■		■		■	■
	$E_{shell}^p$	■		■		■	■
	$E_{pair}^p$	■	■	■		■	■
	$\Delta_p$	■	■	■		■	■
NLSH	$S_{2p}$	■		■		■	■
	$\delta_{2p}$	■	■	■		■	■
	$E_{shell}^p$	■	■	■		■	■
	$E_{pair}^p$	■	■	■		■	■
	$\Delta_p$	■	■	■		■	■
TM1	$S_{2p}$			■		■	■
	$\delta_{2p}$			■		■	■
	$E_{shell}^p$			■		■	■
	$E_{pair}^p$			■		■	■
	$\Delta_p$			■		■	■
TW99	$S_{2p}$	■		■		■	■
	$\delta_{2p}$	■	■	■		■	■
	$E_{shell}^p$	■	■	■		■	■
	$E_{pair}^p$	■	■	■	■	■	■
	$\Delta_p$	■	■	■	■	■	■
DD-ME1	$S_{2p}$			■		■	■
	$\delta_{2p}$	■		■		■	■
	$E_{shell}^p$	■		■		■	■
	$E_{pair}^p$	■	■	■	■	■	■
	$\Delta_p$	■	■	■	■	■	■
PK1	$S_{2p}$	■		■		■	■
	$\delta_{2p}$	■		■		■	■
	$E_{shell}^p$	■	■	■		■	■
	$E_{pair}^p$	■	■	■		■	■
	$\Delta_p$	■	■	■		■	■
PK1R	$S_{2p}$	■		■		■	■
	$\delta_{2p}$	■		■		■	■
	$E_{shell}^p$	■	■	■		■	■
	$E_{pair}^p$	■	■	■		■	■
	$\Delta_p$	■	■	■		■	■

TABLE III: The possible magic neutron number suggested by two-neutron separation energies, two-neutron gaps, shell correction energies, pairing energies and effective pairing gaps for neutron with interactions NL1, NL3, NL-SH, TM1, TW-99, DD-ME1, PK1 and PK1R, respectively.

Effective interactions	Quantity	Magic neutron number candidates										
		138	164	172	184	198	216	228	238	252	258	274
NL1	$S_{2n}$	■		■	■	■		■	■	■	■	■
	$\delta_{2n}$	■		■	■	■		■	■		■	■
	$E_{shell}^n$				■						■	
	$E_{pair}^n$	■	■	■	■	■		■	■	■	■	■
	$\Delta_n$	■	■	■	■	■		■	■	■	■	■
	NL3	$S_{2n}$	■		■	■	■		■	■	■	■
$\delta_{2n}$		■	■	■	■	■		■	■		■	■
$E_{shell}^n$				■	■						■	
$E_{pair}^n$		■	■	■	■	■	■	■	■	■	■	■
$\Delta_n$		■	■	■	■	■	■	■	■	■	■	■
NLSH		$S_{2n}$	■	■	■	■	■	■	■	■	■	■
	$\delta_{2n}$	■	■	■	■	■	■	■		■	■	■
	$E_{shell}^n$		■	■	■					■	■	
	$E_{pair}^n$	■	■	■	■	■	■	■	■	■	■	■
	$\Delta_n$	■	■	■	■	■	■	■	■	■	■	■
	TM1	$S_{2n}$	■		■	■	■		■	■	■	■
$\delta_{2n}$		■		■	■	■		■	■		■	■
$E_{shell}^n$				■	■						■	
$E_{pair}^n$		■	■	■	■	■		■	■	■	■	■
$\Delta_n$		■	■	■	■	■		■	■	■	■	■
TW99		$S_{2n}$	■	■	■	■	■	■	■	■	■	■
	$\delta_{2n}$	■	■	■	■	■	■	■		■	■	■
	$E_{shell}^n$		■	■	■		■				■	
	$E_{pair}^n$	■	■	■	■	■	■	■	■	■	■	■
	$\Delta_n$	■	■	■	■	■	■	■	■	■	■	■
	DD-ME1	$S_{2n}$	■	■	■	■	■		■	■	■	■
$\delta_{2n}$		■	■	■	■	■		■	■		■	■
$E_{shell}^n$				■	■		■				■	
$E_{pair}^n$		■	■	■	■	■		■	■	■	■	■
$\Delta_n$		■	■	■	■	■		■	■	■	■	■
PK1		$S_{2n}$	■	■	■	■	■	■	■	■	■	■
	$\delta_{2n}$	■	■	■	■	■	■	■		■	■	■
	$E_{shell}^n$			■	■						■	
	$E_{pair}^n$	■	■	■	■	■	■	■	■	■	■	■
	$\Delta_n$	■	■	■	■	■	■	■	■	■	■	■
	PK1R	$S_{2n}$	■	■	■	■	■	■	■	■	■	■
$\delta_{2n}$		■	■	■	■	■	■	■		■	■	■
$E_{shell}^n$				■	■						■	
$E_{pair}^n$		■	■	■	■	■	■	■	■	■	■	■
$\Delta_n$		■	■	■	■	■	■	■	■	■	■	■

TABLE IV: The  $Q$  value, the height of the static fission barrier  $B_f^{stat}(ER)$ , the optimal excitation energy  $E_{opt}^*$  and  $C$ -dependent formation cross section  $\sigma$  at  $E_{opt}^*$  for the cold fusion reaction  $^{208}\text{Pb}(^{85}\text{Sr},1n)^{292}120$  and  $^{208}\text{Pb}(^{97}\text{Sr},1n)^{304}120$  with the input from the constrained RMF for effective interactions NL1, NL3, NLSH and TM1

Cold fusion reactions	RMF Interactions	$Q$ [MeV]	$B_f^{stat}(ER)$ [MeV]	$E_{opt}^*$ [MeV]	$\sigma$	
					$\sigma(C_1)$	$\sigma(C_2)$
$^{208}\text{Pb}(^{85}\text{Sr},1n)^{292}120$	NL1	296.51	10.62	14.78	15.8pb	9.5pb
	NL3	302.84	8.15	14.92	1.1pb	720fb
	NLSH	297.88	7.21	13.94	0.26fb	0.16fb
	TM1	296.83	5.74	12.83	0.47fb	0.29fb
$^{208}\text{Pb}(^{97}\text{Sr},1n)^{304}120$	NL1	308.42	12.62	9.96	86.8nb	55.1nb
	NL3	305.09	3.98	9.55	0.64fb	0.40fb
	NLSH	300.37	5.15	10.49	13.8fb	8.6fb
	TM1	299.73	5.51	11.21	20.5fb	12.6fb

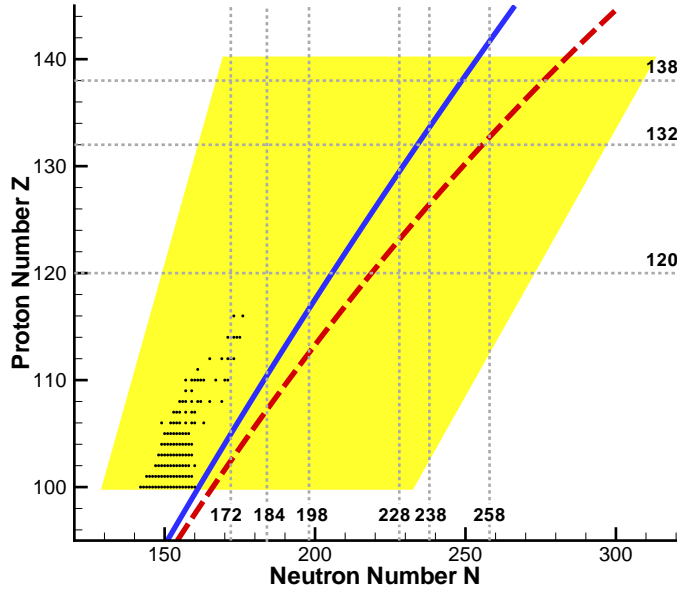
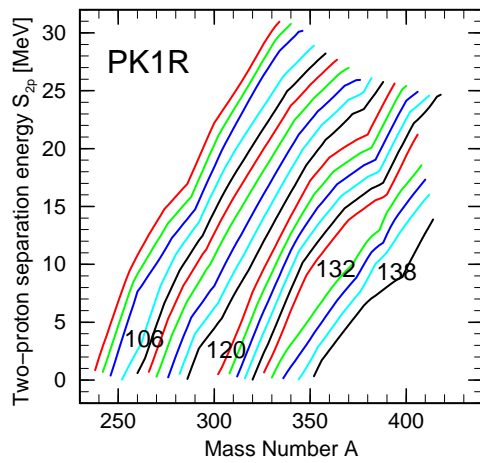
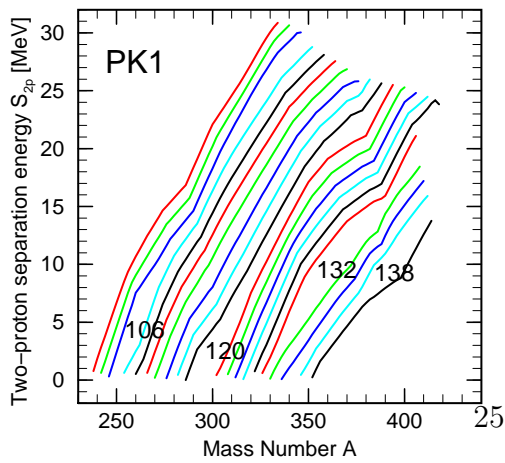
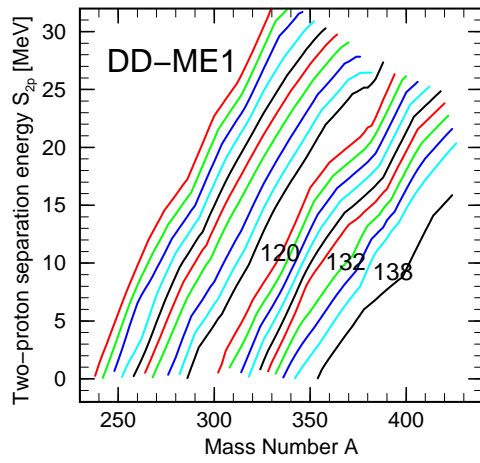
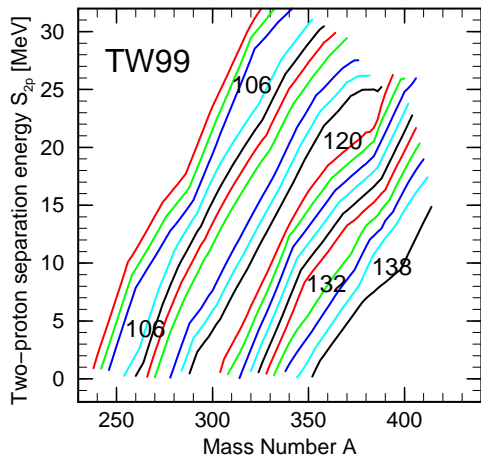
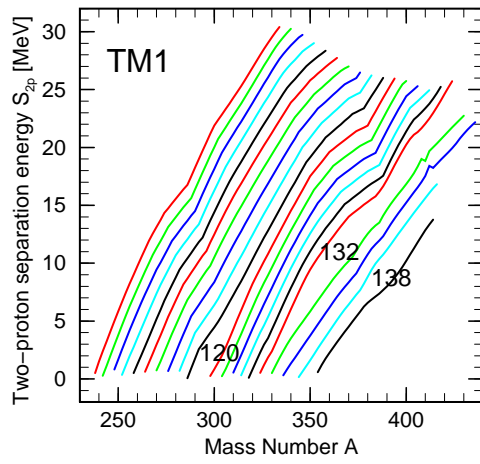
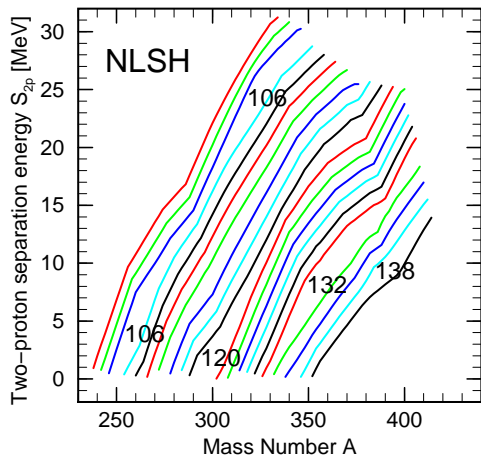
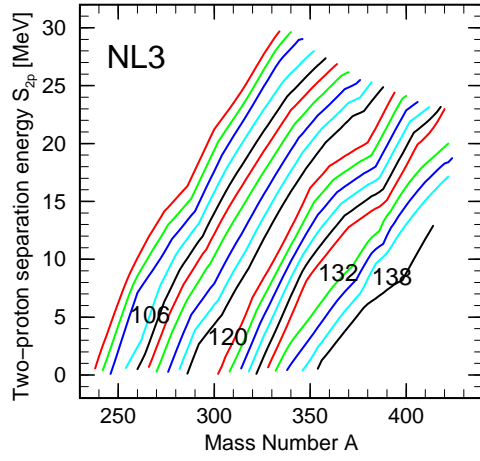
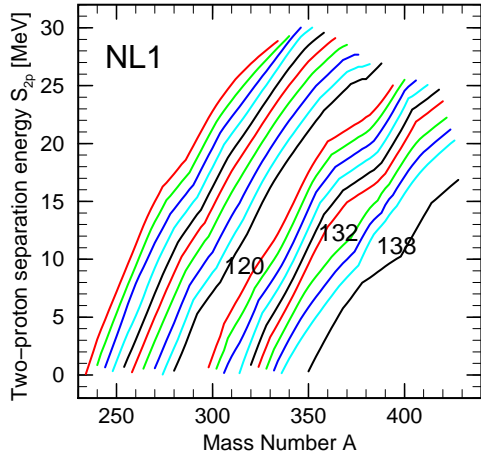


FIG. 1: Nuclear chart in the superheavy region. The long-dashed and solid lines represent the  $\beta$ -stability lines by formula  $N - Z = 6 \times 10^{-3} \cdot A^{5/3}$  [48] and  $Z = \frac{A}{1.98 + 0.0155 \cdot A^{2/3}}$  [49] respectively. The dots lying at the lower-left corner represent the superheavy nuclei observed or declared to be observed experimentally.





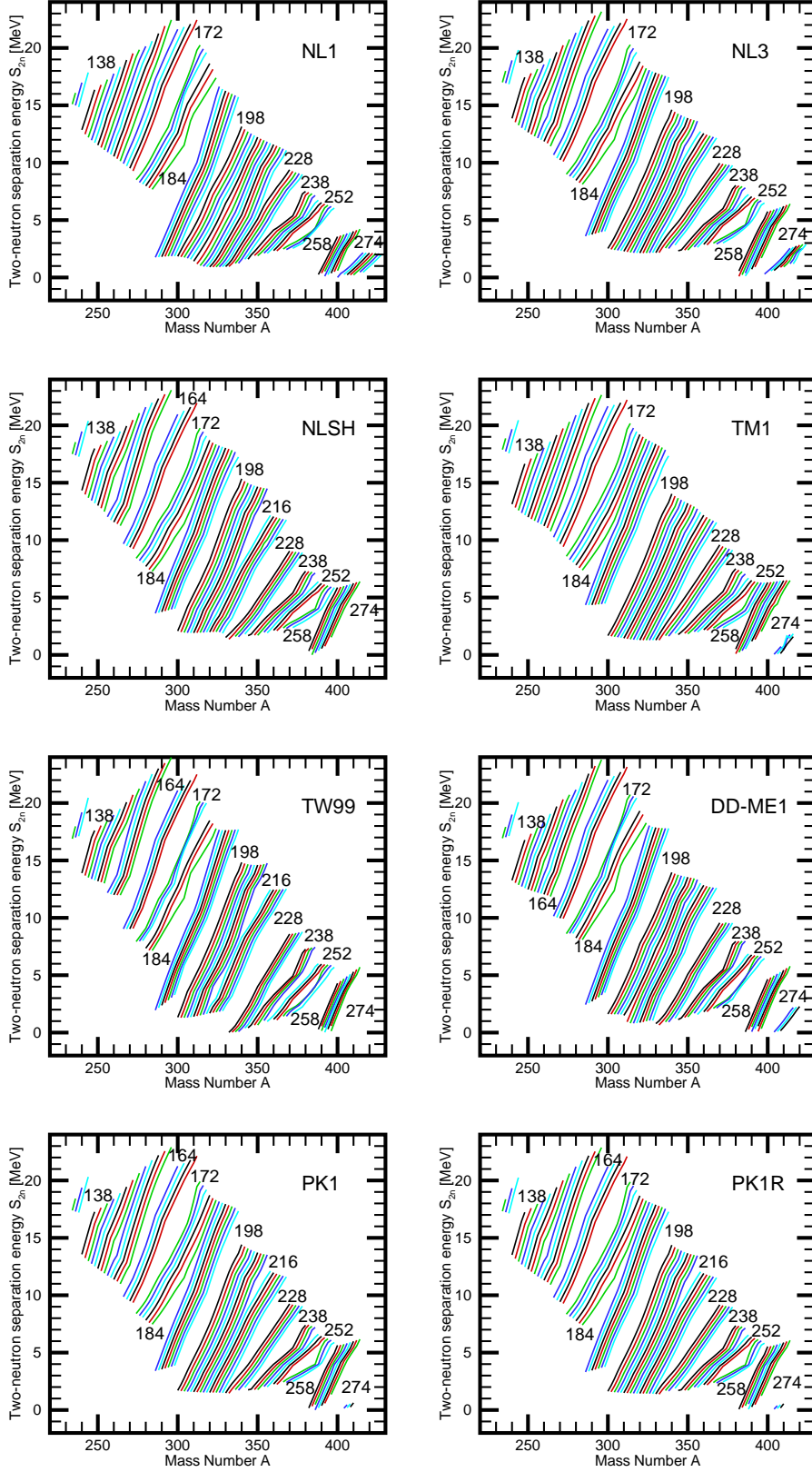


FIG. 3: The two-neutron separation energies  $S_{2n}(N, Z) = E_B(N, Z) - E_B(N - 2, Z)$  as a function of mass number  $A$  obtained by RCHB calculation with effective interactions NL1, NL3, NL-SH, TM1, TW-99, DD-ME1, PK1, and PK1R, respectively.

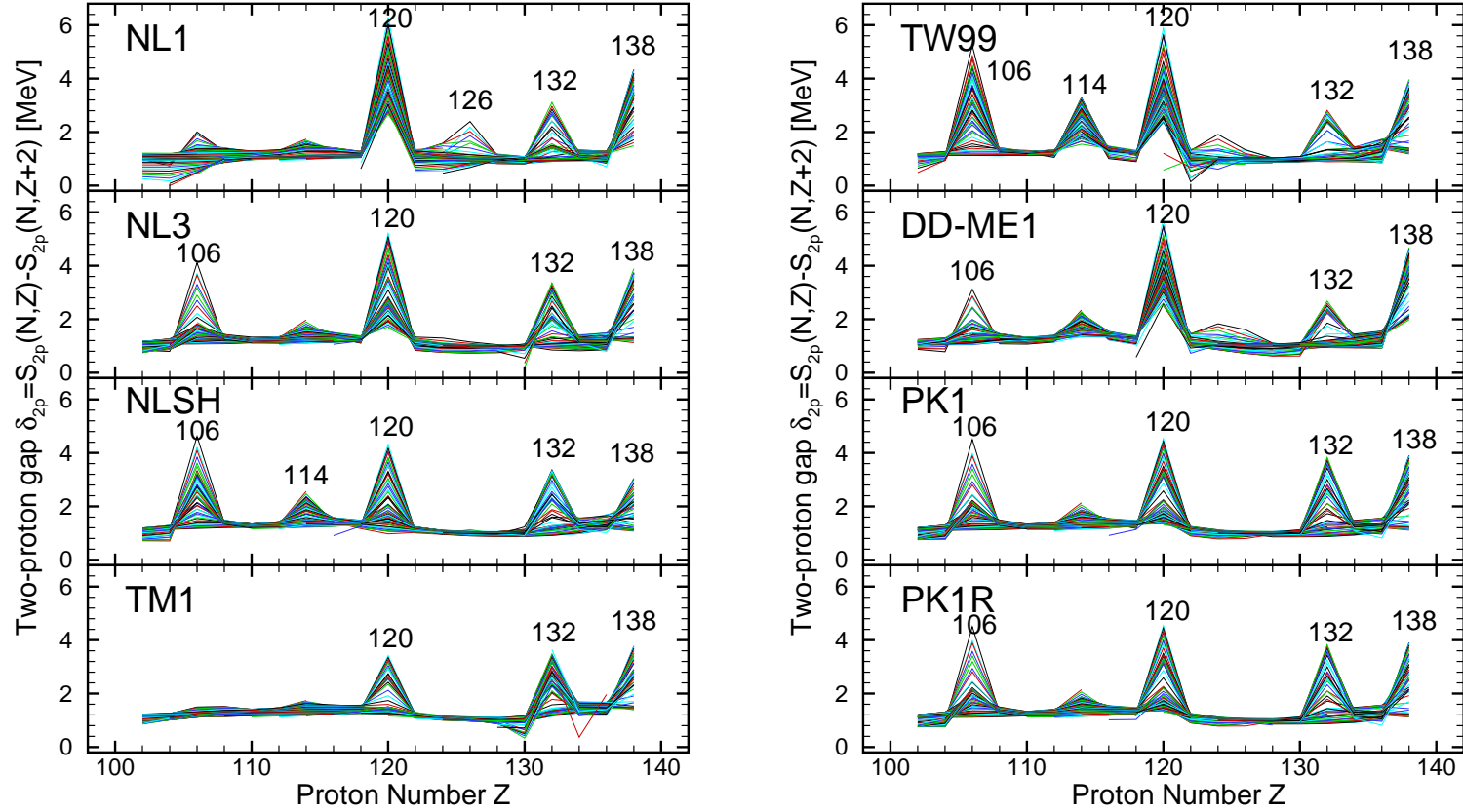


FIG. 4: The two-proton gaps  $\delta_{2p}(N, Z) = S_{2p}(N, Z) - S_{2p}(N, Z + 2)$  as a function of proton number obtained by RCHB calculation with effective interactions NL1, NL3, NL-SH, TM1, TW-99, DD-ME1, PK1, and PK1R, respectively.

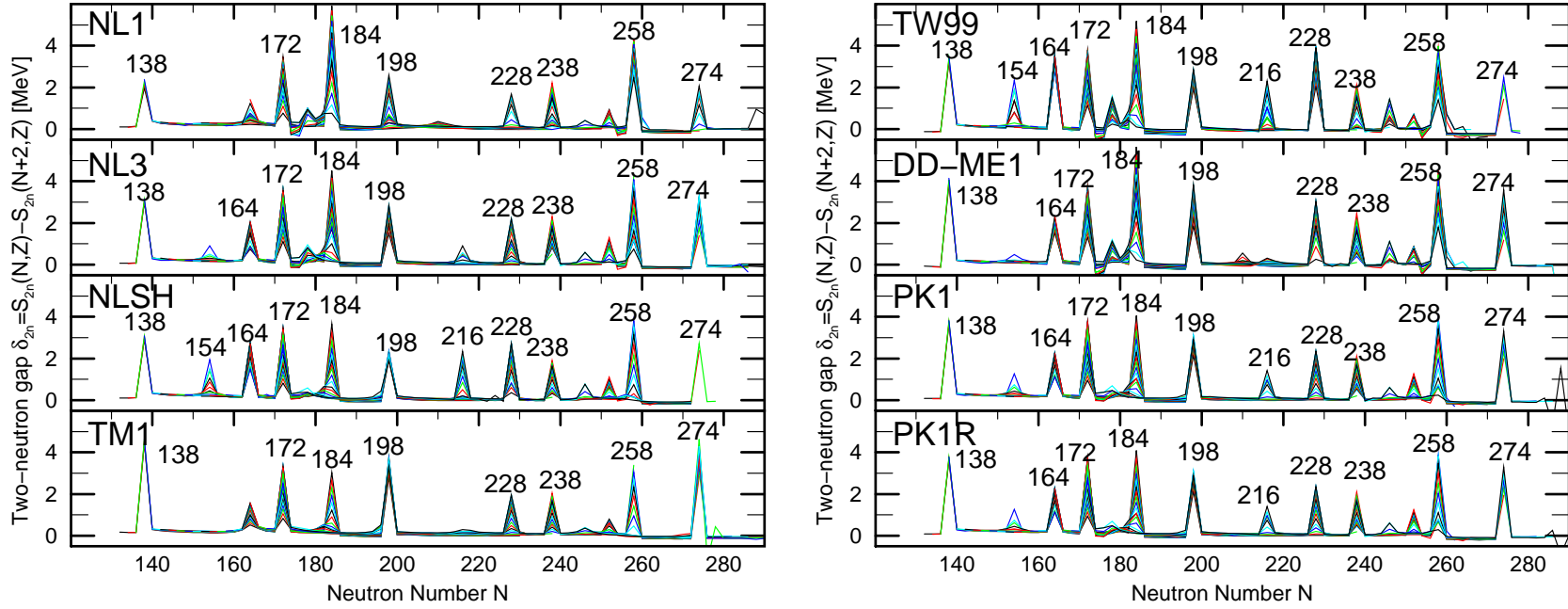


FIG. 5: The two-neutron gaps  $\delta_{2n}(N, Z) = S_{2n}(N, Z) - S_{2n}(N + 2, Z)$  as a function of neutron number obtained by RCHB calculation with effective interactions NL1, NL3, NL-SH, TM1, TW-99, DD-ME1, PK1, and PK1R, respectively.

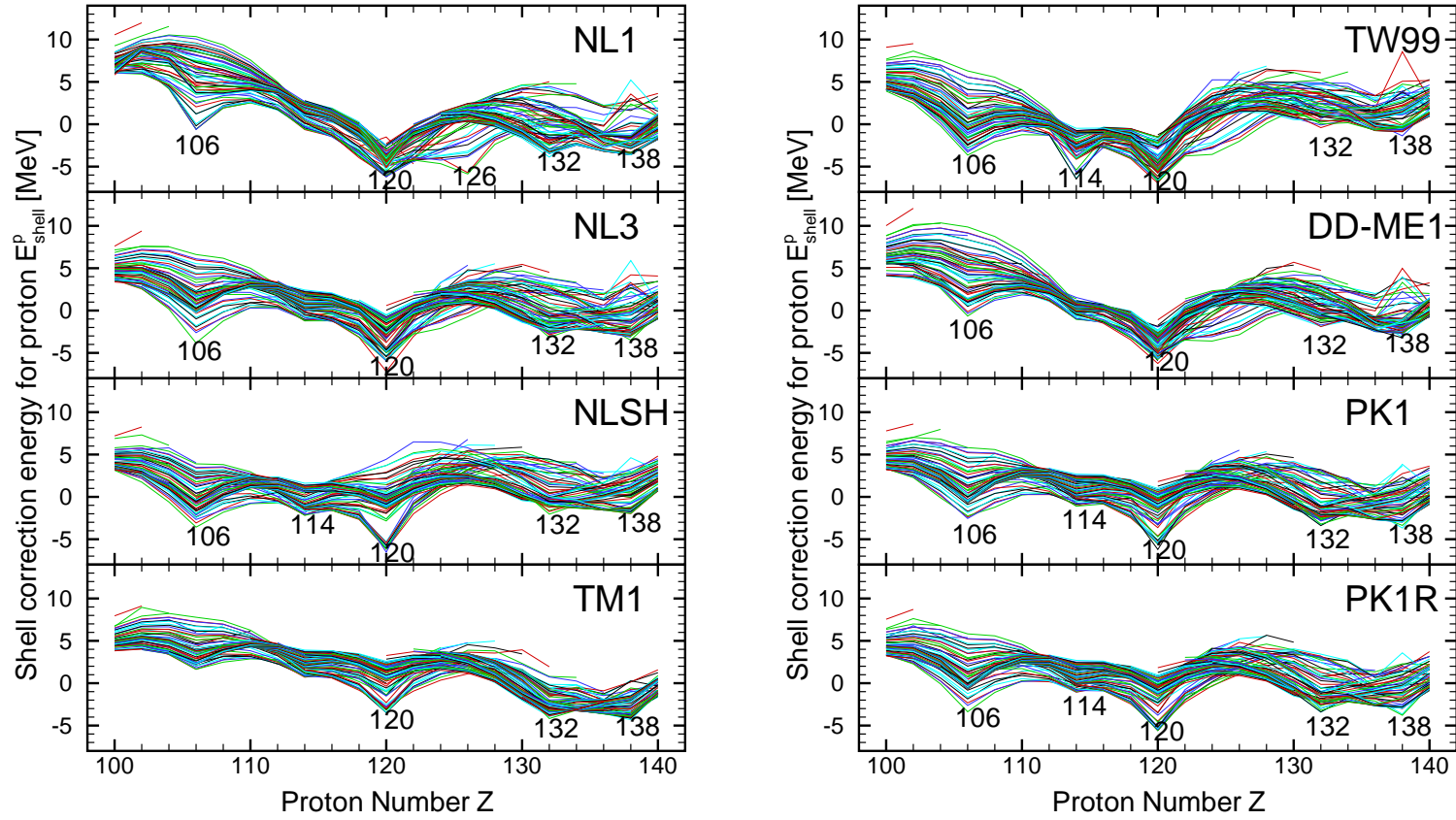


FIG. 6: The shell correction energies for proton  $E_{shell}^p$  as a function of proton number obtained by RCHB calculation with effective interactions NL1, NL3, NL-SH, TM1, TW-99, DD-ME1, PK1 and PK1R, respectively.

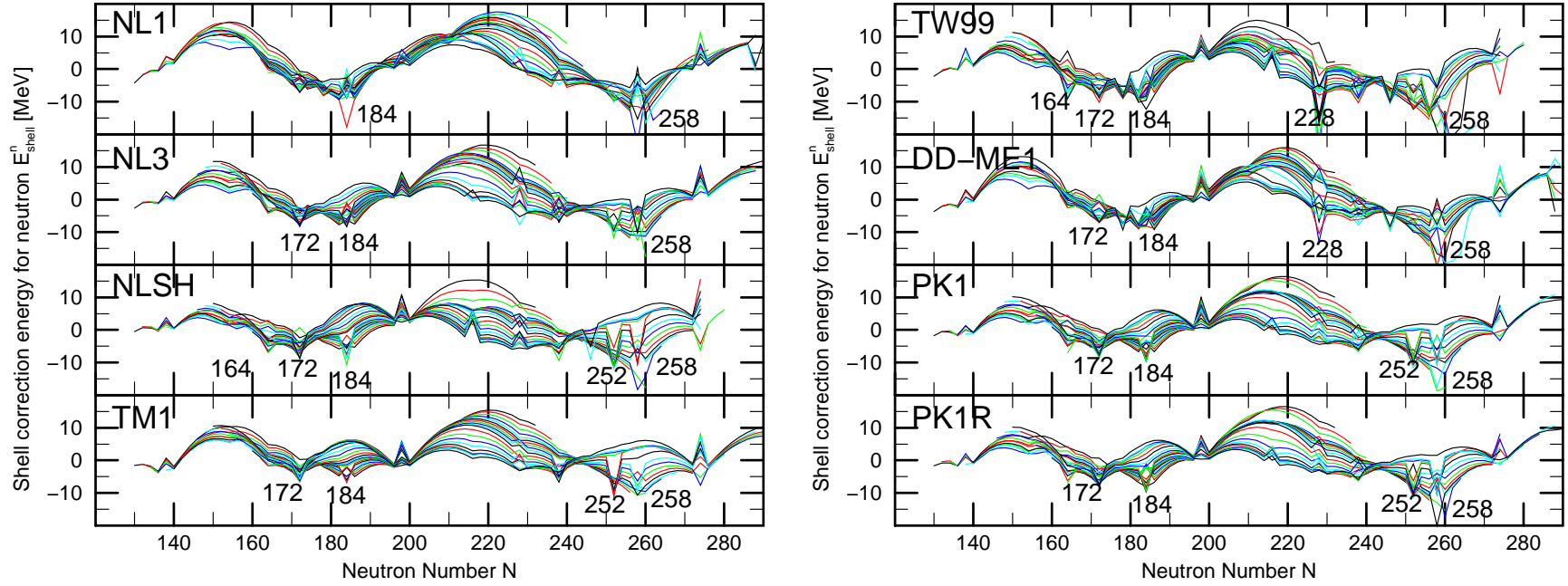


FIG. 7: The shell correction energies for neutron  $E_{shell}^n$  as a function of neutron number obtained by RCHB calculation with effective interactions NL1, NL3, NL-SH, TM1, TW-99, DD-ME1, PK1 and PK1R, respectively.

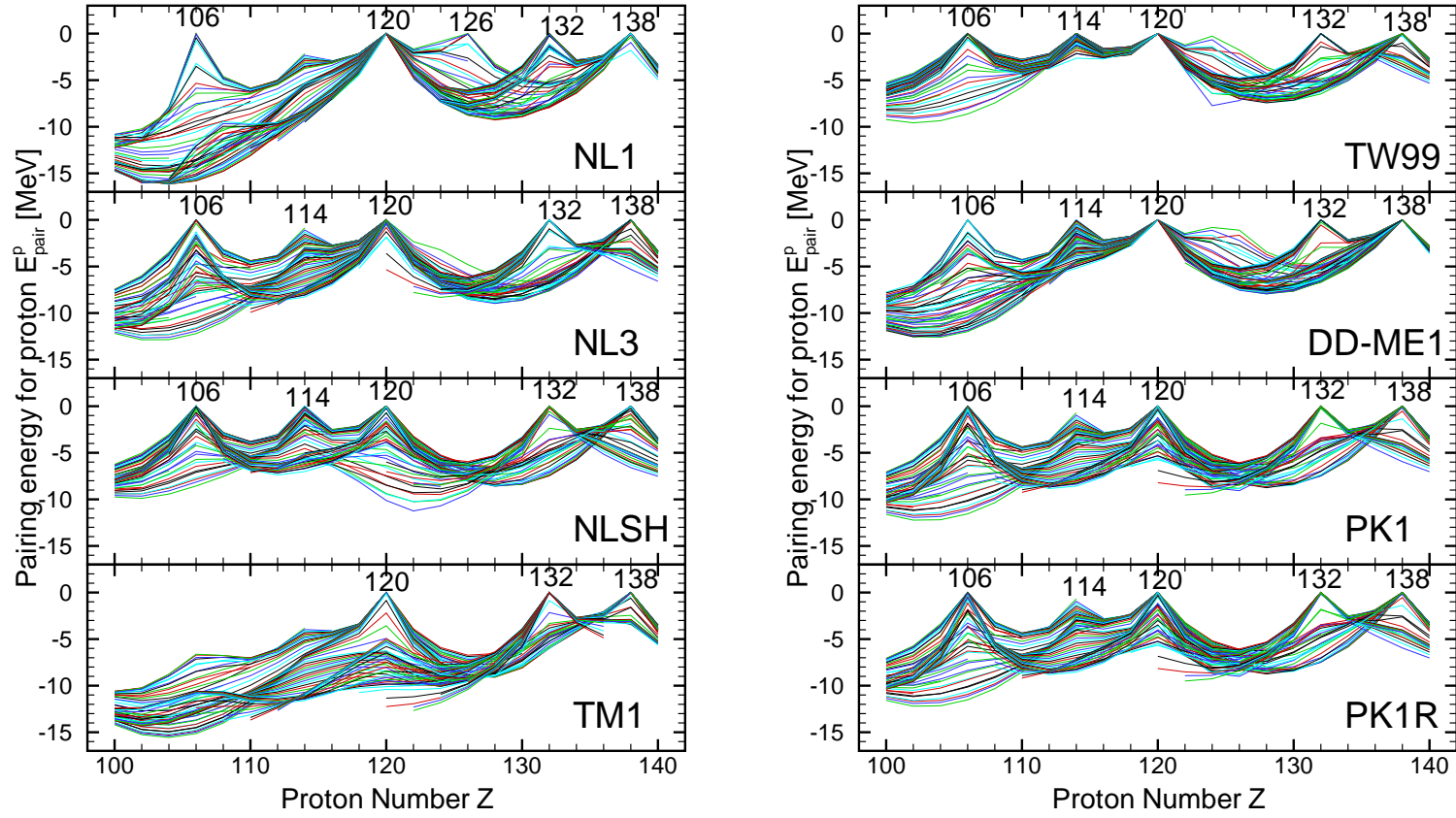


FIG. 8: The pairing energies for proton  $E_{pair}^p$  as a function of proton number obtained by RCHB calculation with effective interactions NL1, NL3, NL-SH, TM1, TW-99, DD-ME1, PK1 and PK1R, respectively.

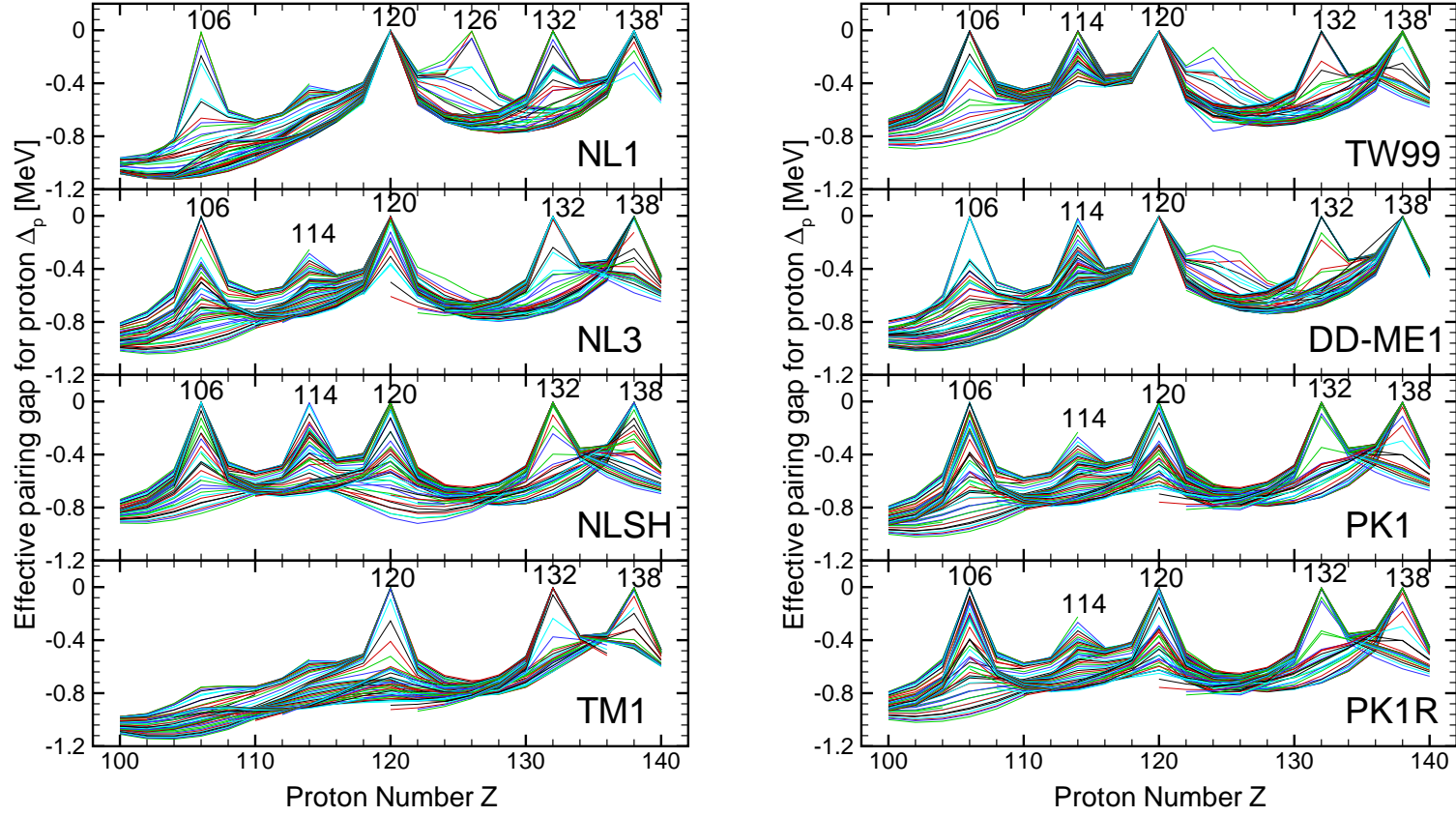


FIG. 9: The effective pairing gaps for proton  $\Delta_p$  as a function of proton number obtained by RCHB calculation with effective interactions NL1, NL3, NL-SH, TM1, TW-99, DD-ME1, PK1 and PK1R, respectively.



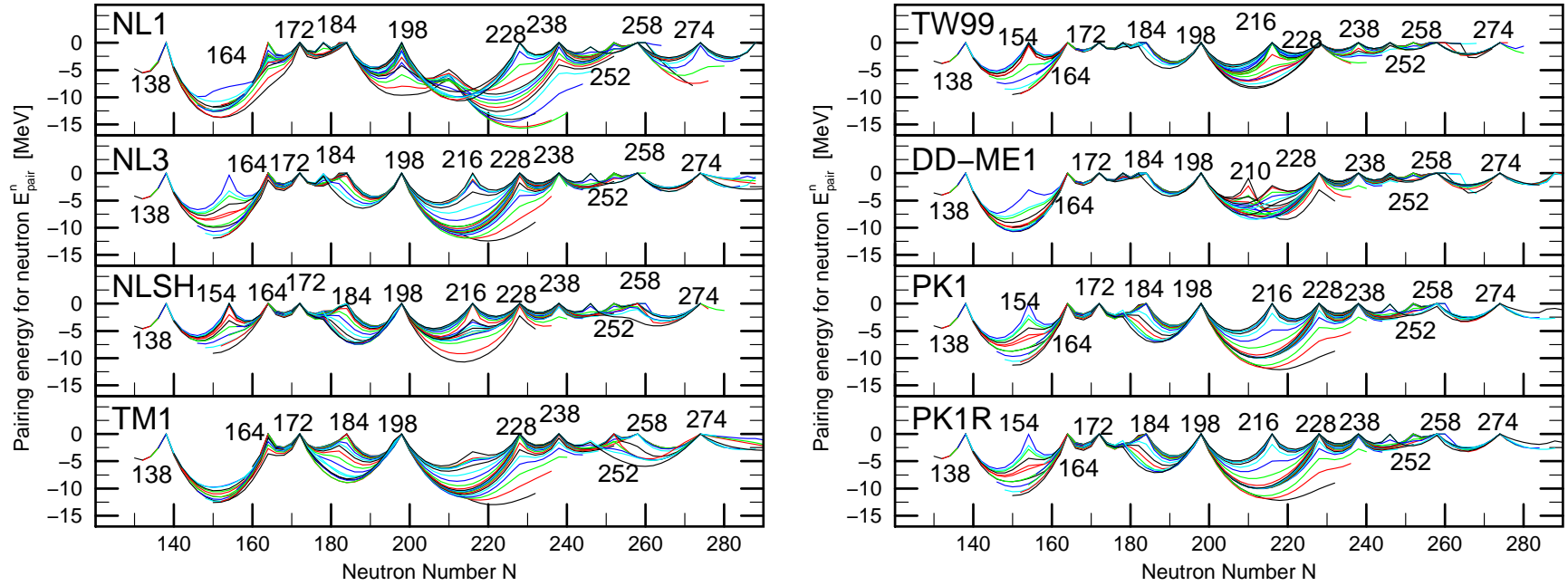


FIG. 10: The pairing energies for neutron  $E_{pair}^n$  as a function of neutron number obtained by RCHB calculation with effective interactions NL1, NL3, NL-SH, TM1, TW-99, DD-ME1, PK1 and PK1R, respectively.

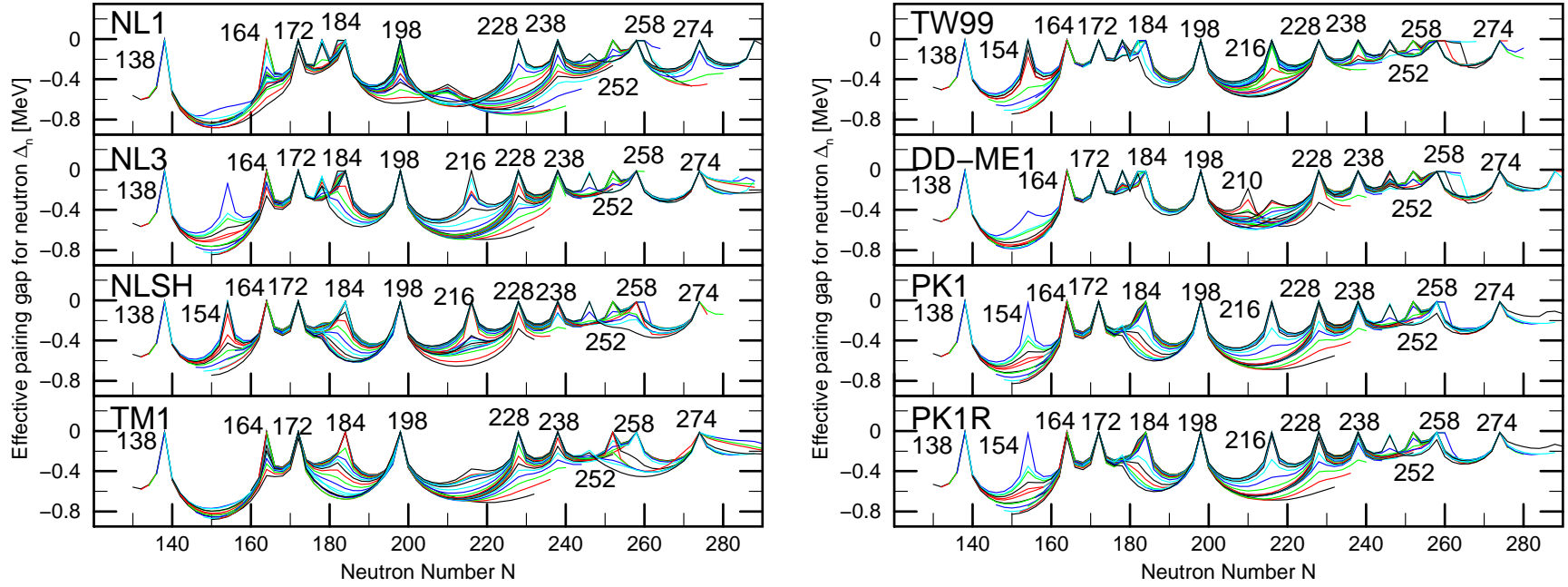


FIG. 11: The effective pairing gaps for neutron  $\Delta_n$  as a function of neutron number obtained by RCHB calculation with effective interactions NL1, NL3, NL-SH, TM1, TW-99, DD-ME1, PK1 and PK1R, respectively.

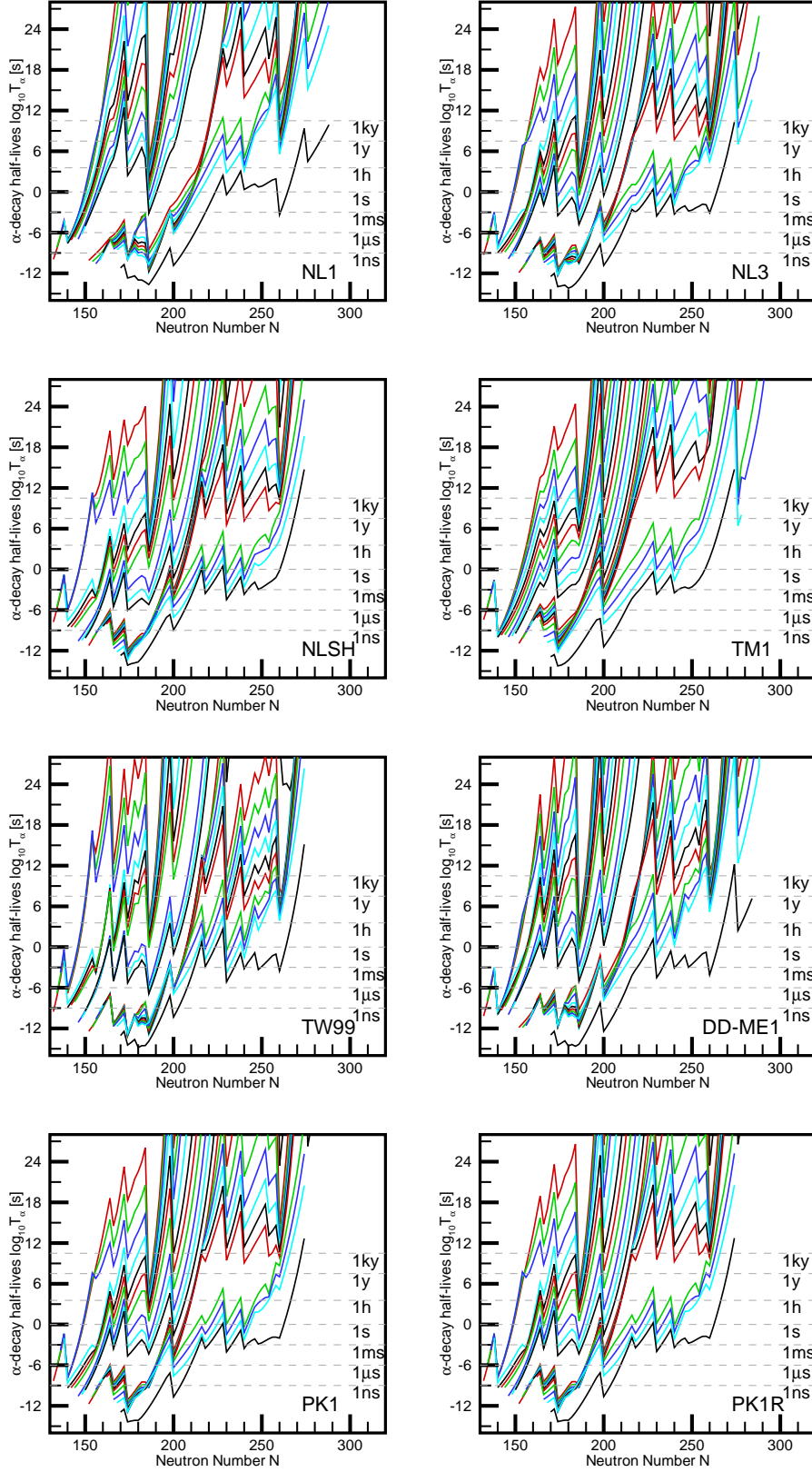


FIG. 12: The  $\alpha$ -decay half-lives  $T_\alpha$  as a function of neutron number obtained by RCHB calculation with effective interactions NL1, NL3, NL-SH, TM1, TW-99, DD-ME1, PK1, and PK1R, respectively.

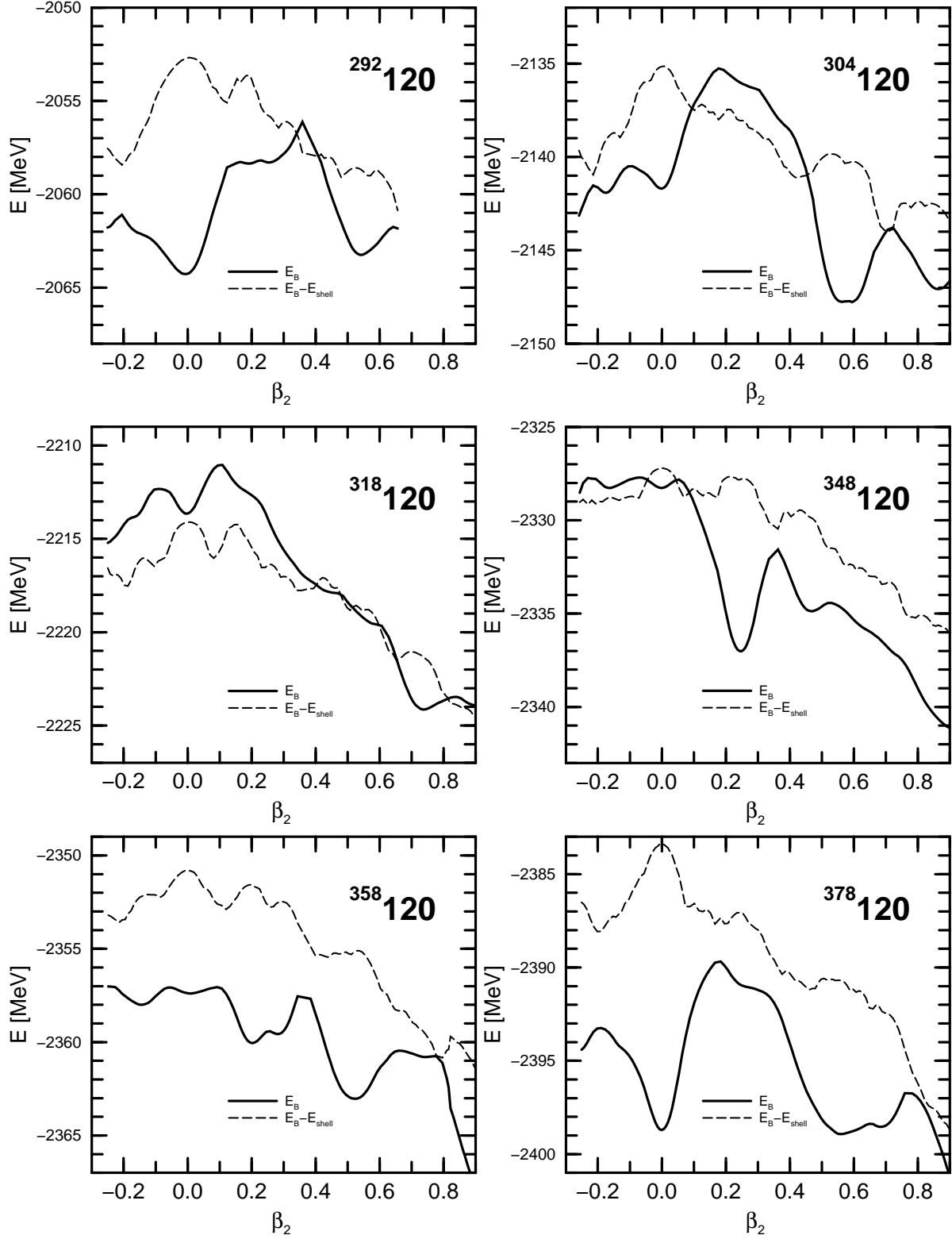


FIG. 13: The binding energy and the equivalent macroscopic energy of  $^{292,304,318,348,358,378}120$  calculated in the constrained RMF theory with effective interaction NL3.

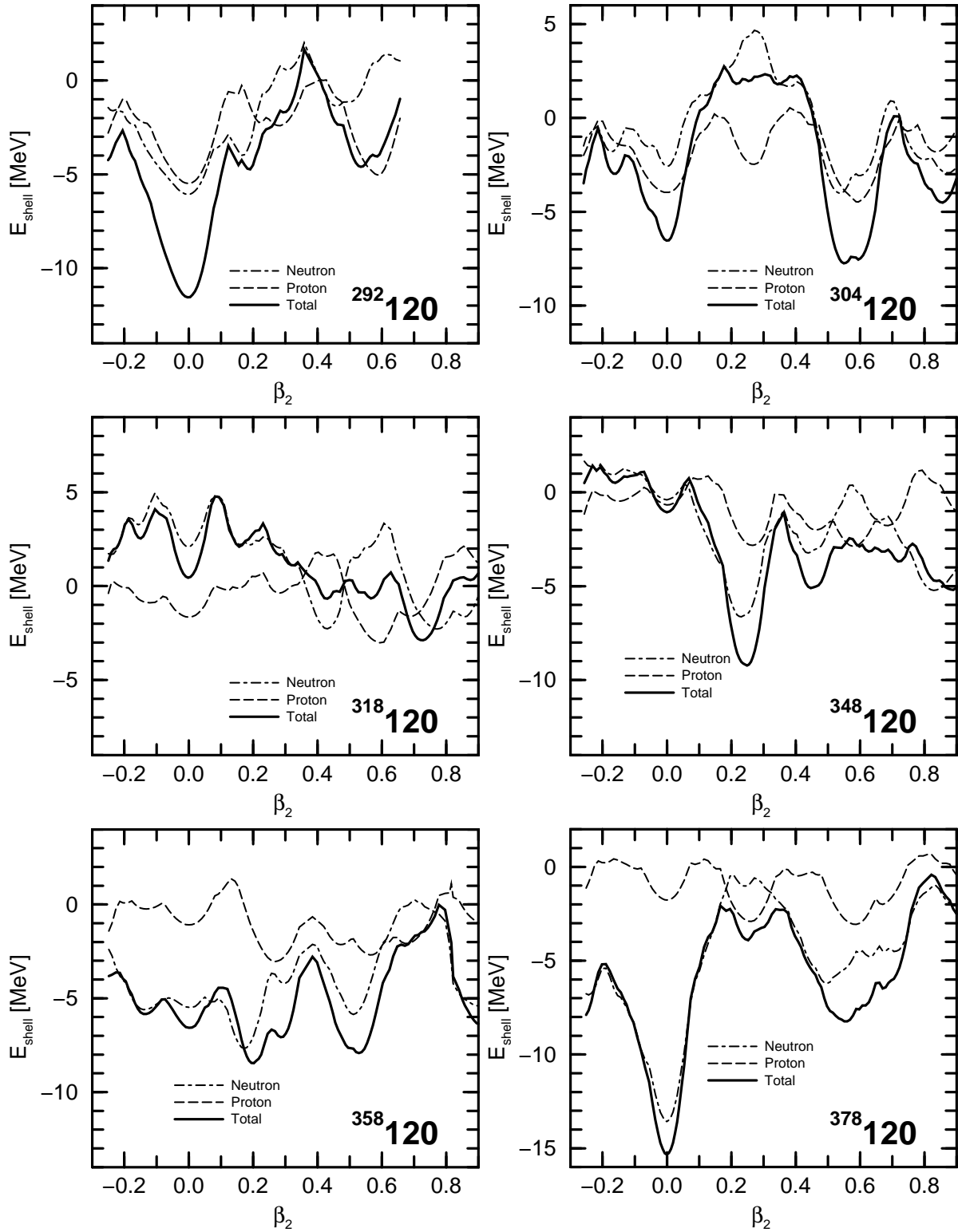


FIG. 14: The shell correction energy of  $^{292,304,318,348,358,378}_{120}$  calculated in the constrained RMF theory with effective interaction NL3.